Journal of Energy Storage 24 (2019) 100755

Contents lists available at ScienceDirect

Journal of Energy Storage

journal homepage: www.elsevier.com/locate/est

# Energy generation and storage by salinity gradient power: A model-based assessment☆

Zohreh Jalili[a,b], Kjersti Wergeland Krakhella[a,b], Kristian Etienne Einarsrud[a], Odne Stokke Burheim[b,*]

[a] Department of Materials Science and Engineering, Norwegian University of Science and Technology (NTNU), NO-7491 Trondheim, Norway
[b] Department of Energy and Process Engineering, Norwegian University of Science and Technology (NTNU), NO-7491 Trondheim, Norway

ARTICLE INFO

*Keywords:*
Energy storage
Electrodialytic energy storage system
Osmotic energy storage system
Capacitive energy storage system
Concentration battery efficiency

ABSTRACT

Three energy storage systems based on mixing and desalination of solutions with different salt concentrations are presented, namely, reverse electrodialysis, pressure retarded osmosis and capacitive Donnan potential, coupled to their corresponding desalination technologies: electrodialysis, reverse osmosis and membrane capacitive deionisation.

Conceptual mathematical models are used to assess power densities and efficiency, and to address the influence on the performance of factors such as temperature and residence time. The maximum power densities for electrodialysis, osmotic and capacitive energy storage systems are calculated as 4.69, 4.83 and 0.503 $W\,m^{-2}$, respectively, at 25 °C and residence time of 20 s, corresponding to an average fluid velocity of 5 mm/s. In order to achieve competitive economic energy (in the EU) with this power density, the membrane price needs to be lower than 2.9, 3.0 and 0.31$ $m^{-2}$, for each of the technologies. Utilisation of waste heat to increase the temperature to 60 °C increases the power density to 8.54, 6.04 and 0.708 $W\,m^{-2}$, which allows for 25% higher osmotic membrane price (3.7$ $m^{-2}$), and over 80% and 40% higher price (5.2 and 0.43$ $m^{-2}$) for the ionic exchange membrane used in the electrodialytic and capacitive energy storage system respectively, while still having economic energy production. Advantages and disadvantages of the proposed energy storage systems are discussed, along with the cost evaluation for each technology.

## 1. Introduction

In order to secure a more sustainable energy supply, reduce carbon emissions and dependency of fossil fuels, renewable energy sources have received considerable attention in research and industrial developments over the last decades. Significant technological improvements have been made, enabling energy production utilising wind, solar, tidal, geothermal and salinity gradient power sources (SGP) [1–4]. A study and forecast made by DNV-GL [5] on the global energy production from 2015 to 2050 is shown in Figure 1.

Fig. 1 indicates a steady increase in energy production and that the growth mainly will be in photovoltaics and wind, both of which depend on large-scale storage due to their intermittent nature [6]. Large-scale energy storage is also expected to play a role in resolving issues related to peak energy consumption and production typically being out of phase. Fig. 2 shows the net electric load (electricity demand minus the renewable energy supply) for the California grid system operator, with forecasts for 2020 [7]. Data for 2012 and 2013 indicate that the energy demand has two distinct peaks, one in the morning and one during the evening. Following 2014, the net energy demand is decreasing during the daytime, due to increased photovoltaic capacity, resulting in the so-called duck curve [7]. Extrapolating beyond 2020 it is possible to imagine a potential over the generation of energy during daytime hours, followed by an abrupt ramp in demand during the evening.

Energy storage is a viable solution for smoothing out the duck curve, allowing for energy to be generated when it is available and dispatched when and where it is needed. Despite recent advances in battery technology for small and medium scale applications, achieving low cost, high-efficiency large-scale energy storage systems with long life cycles remains a challenge [8,9]. Energy storage based on salinity gradients can potentially overcome some of these challenges.

The energy that can be stored in solutions with different salinity can

☆ Jalili and Krakhella have equal collaboration in writing of this article.

* Corresponding author.
*E-mail addresses:* zohreh.jalili@ntnu.no (Z. Jalili), kjersti.s.krakhella@ntnu.no (K.W. Krakhella), kristian.e.einarsrud@ntnu.no (K.E. Einarsrud), odne.s.burheim@ntnu.no (O.S. Burheim).

https://doi.org/10.1016/j.est.2019.04.029
Received 7 August 2018; Received in revised form 10 April 2019; Accepted 29 April 2019
Available online 11 June 2019

**Nomenclature**

| | |
|---|---|
| $\alpha$ | membrane permselectivety |
| $N_m$ | number of membranes |
| $F$ | Faraday constant |
| $A_m$ | membrane area |
| $\Delta\pi$ | osmotic pressure |
| $R$ | universal gas constant |
| $T$ | temperature |
| $\Delta P_h$ | hydrostatic pressure |
| $\rho$ | density |
| $\rho_c$ | conductivity concentrated solution |
| $\rho_d$ | conductivity dilute solution |
| $Re$ | Reynold number |
| $K_w$ | permeability of membrane respect to the water |
| $J_w$ | water flux across the membrane |
| $c_d$ | concentration for dilute solution |
| $c_c$ | concentration for concentrated solution |
| $E_{OCP}$ | open circuit potential |
| $i$ | current density |
| $R_\Omega$ | ohmic resistance |
| $R_{AEM}$ | ohmic resistance in AEM |
| $R_{CEM}$ | ohmic resistance in CEM |
| $\beta$ | shadow factor of the spacer on the membranes |
| $h_d$ | height of the dilute flow channel |
| $h_c$ | height of the concentrated flow channel |
| $\epsilon$ | porosity spacer |
| $P$ | power density |
| $\mu$ | viscosity |
| $l$ | length flow channel |
| $t_{res}$ | residence time |
| $d_h$ | hydraulic diameter |
| $S_{sp}$ | surface of the spacer filaments |
| $V_{sp}$ | volume of the spacer filaments |
| $W$ | work density |
| $\eta$ | efficiency |
| $E_{Donnan}$ | the Donnan potential |
| $E_c$ | capacitive potential |
| $E_{c,0}$ | start capacitive potential |
| $t$ | time |
| $C$ | capacitance of porous electrodes (MCDI and CDP) |
| $R_{electrode}$ | resistance porous electrodes (MCDI and CDP) |
| $t_{cycle}$ | cycle time for MCDI and CDP |
| $m_m$ | mass salt transported through membrane |

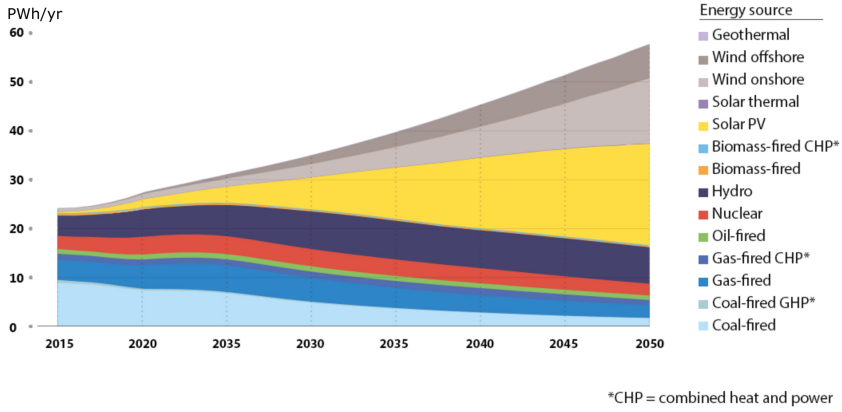


**Fig. 1.** Forecast of global energy production towards 2050 as of DNV-GL [5].

be significant, depending upon the relative salt concentrations. For instance, the energy released when mixing river- and seawater is around 2 kJ/l of river water, approximately equivalent to a 200 m head of water [1,10]. In that perspective, the energy potential is comparable to that from pumped hydro [2]. Harvesting this energy by membrane-based techniques such as reversed electrodialysis (RED), pressure retarded osmosis (PRO) and capacitive Donnan potential (CDP) has been described by several authors, demonstrating the potential for power generation [1–4,11–17]. For a system consisting of 0.5 and 0.05 M NaCl solutions, Post et al. [2] demonstrated maximum power densities of over 2.0 W m$^{-2}$ for RED and 1.2 W m$^{-2}$ for PRO, albeit with similar average power densities due to differences in discharge times. The power density of CDP is expected to be lower, 0.05 W m$^{-2}$ as of Hatzell et al. [15].

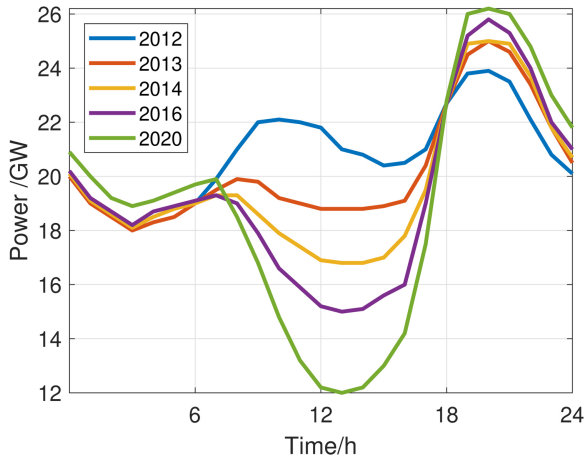


**Fig. 2.** California net electricity load requirement [7] with forecasts for 2020.

Combining SGP technologies with corresponding desalination technologies allow for scalable and sustainable energy storage, as proposed by Yip et al. [18]. Kingsbury et al. [8] and Egmond et al. [19] have both demonstrated a concentration battery based on (reverse) electrodialysis ([R]ED), a concept further developed by Li et al. [20], demonstrating the potential for large-scale storage. An alternative has been proposed by Skilbred et al. [21], suggesting an energy storage system based on RED as a hydrogen production unit, combined with precipitation and evaporation for desalination, with a maximum power density of 28.1 W m$^{-2}$ using $KNO_3$ at 40 °C. Raka et al. conducted an economic study of hydrogen production with RED and ammonium bicarbonate finding an upper limit for the membrane cost of 20 €/m2 [94].

Enhanced performance relies upon further development in membrane technology as well as optimising system chemistry and geometry.

However, as each of the technologies considered have been developed separately for other applications than energy storage, optmisation has so far been done only for specific technologies and not for combinations. Considering for instance reverse osmosis (RO), the membrane must have high salt rejection while an optimised membrane for PRO should have high water permeation. Since the premises for salinity gradient energy storage is to produce power in high demand periods and utilise cheap electricity when demand is low, optimisation with respect to PRO is more critical than RO, as long as the salt rejection does not become so low that separation in RO is impeded.

For energy storage systems based on ED-RED, the principal focus should be on system characteristics such as stack resistivity [22,4,23], closely related to flow conditions. As demonstrated in simulations by Jalili et al. [24], flow promoters in the dilute solution channels reduce the stack resistivity, while the opposite effect was found in the concentrated channel.

Capacitive systems, i.e. membrane capacitive deionisation (MCDI) and CDP are also strongly influenced by flow conditions, in particular with regard to phenomena related to the inherent switching between concentrated and diluted streams [25,26].

Each of technologies considered are to some extent influenced by concentration polarisation, which reduces mass transport rate through the membranes [27–29] and thereby also the attainable power density. The influence of concentration polarisation was investigated with respect to water flux and power density for PRO by Achilli et al. [30]. The maximum power density was 10.2 $W\,m^{-2}$ for a system with 1.02 and 0.04 M NaCl solutions when concentration polarisation was neglected, and 6.2 $W\,m^{-2}$ when included. Corresponding effects have been identified by several authors [31–37] indicating that concentration polarisation reduces the efficiency of PRO by at least 30%. Changing the solutions into hypersaline solutions increases the energy densities, potentially overcoming energy losses and costs, but such salinities requires further advances in the membrane design. For RED additional losses occur due to co-ion transport and electro-osmosis, most notably at low current densities [4].

Pretreatment of water and bio-fouling are the other practical and operational challenges that have to be considered in membrane-based technologies, as well as reduced membrane lifetime due to high salinity [38,39]. Fouling is considered less relevant for the closed systems considered here.

The present work aims to present conceptual mathematical models of three closed salinity gradient energy storage systems (SGES); ED-RED, RO-PRO and MCDI-CDP, allowing for parametric studies of how parameters such as concentration, residence time or temperature impact on the system performance, i.e. peak power densities. A round-trip efficiency will be calculated for each proposed energy storage system to compare the performance and operational ranges. Also, applicability will be identified, and scientific challenges will be highlighted, aiming to describe system specific challenges rather than challenges related to isolated technologies.

## 2. Principles of salinity gradient energy storage

A general schematic of an SGES is shown in Fig. 3, in which darker colours indicate higher concentrations. In a closed system, the concentration difference out of the cell stack is not dissipated, but fed back into the reservoirs, an essential advantage of SGES, improving the efficiency compared to salinity gradient energy.

In order to arrive at a model framework in which the different technologies can be compared, the following assumptions were made:

1. The concentration range is limited up to 1 M, considering the range of concentration of ions in river/freshwater and seawater. Egmond et al. [19] showed that there is an additional energy loss in RED because of osmotic water transport for concentrations > 1 M NaCl. Consequently, 1 M is chosen for the maximum concentration in the concentrated solution channel. As the system is considered to be closed, the sum of concentrations in dilute and concentrated streams is always 1 M, i.e. concentrations are varied from 0.01 M to 0.5 M for the dilute solution and from 0.99 M to 0.5 M for the concentrated solution.
2. The power consumption related to pumping of the solutions is assumed to be identical for all three systems, as described below.
3. The solutions are assumed to be ideal, and concentrations are used rather than activity coefficients. The impact of this assumption is investigated in Appendix B, showing that power densities at most are changed by 16%.
4. Membranes are assumed to be semi-ideal in the sense that salt transport through RO-PRO membranes, and water transport through the ED-RED and MCDI-CDP membranes is neglected.
5. Concentration polarisation is not considered in the current work model for all different types of the studied concentration energy storage system. Although the effect of polarisation is considerable, resulting in at least 30% loss in efficiency [32], it is expected that losses are similar for all three technologies – thus not influencing the comparison.
6. The influence of fouling is neglected as the system is considered to be closed.
7. The membrane selectivity is assumed to be temperature and concentration independent as data for his dependency is scarce in our concentration region of operation [40].
8. The models developed consider only a unit cell, and losses which do not scale linearly with the number of unit cells are not considered (e.g. electrode losses for ED-RED).
9. The remaining losses are assumed to be proportional to the relevant membrane fluxes, i.e. current density in ED-RED and MCDI-CDP (Ohmic losses) and water flux in RO-PRO.
10. The energy demand is shown in Fig. 2 is assumed to be representative of the current case, implying that the peak energy demand occurs over a shorter time period than that of low demand. This is interpreted as a constraint on fluxes related to charging and discharging – the flux related to charging is assumed to be half of

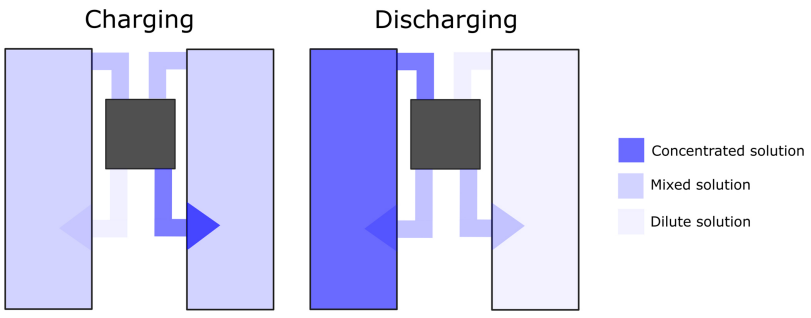


**Fig. 3.** The figure shows a schematic diagram of the concentration energy storage system. While charging (left), energy is stored in the form of chemical potential by creating low and high salinity solutions. While discharging (right), two feed solutions with different concentrations are mixing, and energy is produced.

that related to discharge.

For each of the proposed technologies, the (ideal) driving force $\mathcal{E}_i^{\text{drive}}$ (e.g. potential or pressure), in combination with resistance $\mathcal{R}_i$ and flux $\mathcal{F}_i$ gives a power density on the form

$$P_i = \mathcal{E}_i^{\text{drive}}\mathcal{F}_i \pm \mathcal{R}_i\mathcal{F}_i^2, \tag{1}$$

where '+' is used when charging and '−' when discharging the system. Differentiation with respect to the flux allows for determination of the peak power density, $P_i^{\text{peak}}$, as well as the corresponding flux, $\mathcal{F}_i^{\text{peak}}$. Fluxes and driving forces are used to define a reversible power density,

$$P_i^{\text{rev}} = \mathcal{E}_i^{\text{drive}}\mathcal{F}_i, \tag{2}$$

which is interpreted as the theoretical maximum power density, used as a normalisation factor to determine efficiencies.

The pump power density can be obtained by Eq. (3) as a function of the solution viscosity, $\mu$, hydraulic diameter of the compartments, $D_{\text{h}}$ and residence time, $t_{\text{res}}$, of solutions flowing in the channels [41]:

$$P_{\text{pump}} = f_{\text{pump}}\frac{48\mu l^2 h\epsilon}{t_{\text{res}}^2 d_{\text{h}}^2} \tag{3}$$

In the above equation, $l$ and $h$ are the length and height of the flow channel respectively, and $f_{pump}$ is a factor accounting for the electrical efficiency of the pump, set to 1.5 based on the study by Daniilidis et al. [42] for a RED system. The average flow velocity is given as $\bar{u} = l/t_{\text{res}}$.

The viscosity of the solution, $\mu$ (Pa s), is defined as [43]:

$$\mu = 1.234 \times 10^{-6} e^{0.00212c\,\text{M}+1965/T}, \tag{4}$$

where $c$ is given in M, $T$ is the temperature in Kelvin, and $M$ is the molar mass. Finally, the hydraulic diameter of the channel is defined as [41]:

$$d_{\text{h}} = \frac{4\epsilon}{2/h + (1-\epsilon)(\frac{S_{\text{sp}}}{V_{\text{sp}}})}, \tag{5}$$

where $\frac{S_{\text{sp}}}{V_{\text{sp}}}$ is the ratio between the surface and volume of the spacer filaments.

The energy density, $W_i$, is calculated by integrating the power density with respect to the time:

$$W_i = \int_0^t P_i(t)\text{d}t = \bar{P}_i\Delta t, \tag{6}$$

where $\bar{P}$ is the average power density and $t$ is the total processing time. The energy densities are used to determine the efficiencies of charging by process $i$ and discharging by process $j$, as well as corresponding round-trip efficiency for the combined process $ij$:

$$\eta_j^{\text{charge}} = \frac{W_j^{\text{rev}}}{W_{\text{pump}} + W_j} \tag{7}$$

$$\eta_i^{\text{discharge}} = \frac{W_i^{\text{peak}} - W_{\text{pump}}}{W_i^{\text{rev}}} \tag{8}$$

$$\eta_{\text{ij}}^{\text{round-trip}} = \eta_j^{\text{charge}}\eta_i^{\text{discharge}} = \frac{W_i^{\text{peak}} - W_{\text{pump}}}{W_{\text{pump}} + W_j}\left(\frac{W_j^{\text{rev}}}{W_i^{\text{rev}}}\right) \tag{9}$$

In the following sections, application specific derivations are given for each of the systems considered.

### 2.1. Electrodialytic energy storage system; ED-RED

A schematic of an electrodialytic energy storage system is shown in Fig. 4. Charging is performed by ED, while the corresponding discharging process is performed by RED.

Electrodialysis is a membrane-based demineralisation process realised by an imposed electric potential. The conventional ED system consists of a series of anion and cation-exchange membranes (AEM and CEM) alternately placed between two electrodes. A cell pair (unit cell) is the assembly of a CEM, a concentrated solution compartment, an AEM and a dilute solution compartment. In industrial applications, an ED stack consists of 100–200 cell pairs [44].

In a RED cell, ion-exchange membranes separate the channels in which concentrated and dilute solutions are fed in an alternating pattern. Anions migrate through the AEM towards the anode and cations move through the CEM towards the cathode. As a result of the migration of cations and anions in opposite directions, a net ionic current is produced. Simultaneously, the chemical potential difference between the concentrated and dilute solutions generates a voltage across each membrane. Thus, a portion of the Gibbs free energy of mixing is converted to electrical energy and can be harvested continuously [1,22].

#### 2.1.1. Charging the electrodialytic energy storage system

Charging of the electrodialytic energy storage system occurs through the movement of ions from the dilute to the concentrated solution. The driving force opposing this transport is the open circuit potential, $E_{\text{OCP}}$, given as [45,8]:

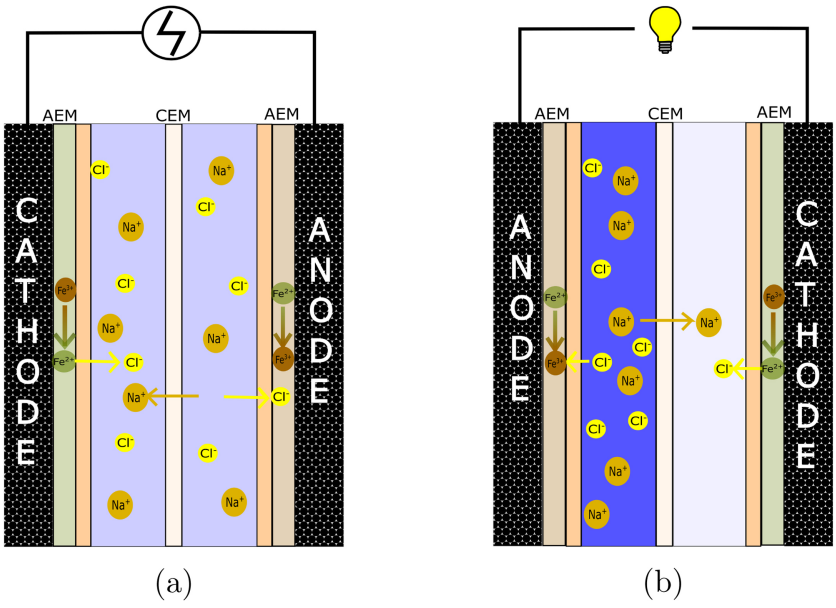


**Fig. 4.** The figure shows a schematic of the electrodialytic energy storage system. (a) During charging by ED, ions move from dilute solution towards the concentrated solution. (b) During discharging by the RED process, the electrical current is reversed, and ions move back from the concentrated to dilute solution, eventually re-establishing the initial condition.

$$\mathcal{E}_{\mathrm{ED/RED}}^{\mathrm{drive}}=E_{\mathrm{OCP}}=2N_m\frac{\bar{\alpha}\mathrm{RT}}{F}\ln\left(\frac{c_{\mathrm{c}}}{c_{\mathrm{d}}}\right), \tag{10}$$

where $c_{\mathrm{c}}$ and $c_{\mathrm{d}}$ are concentrations of the concentrated and dilute solutions respectively, $F$ is Faraday's constant, $T$ is temperature, $R$ is the universal gas constant, $N_m$ is number of membrane pairs and $\bar{\alpha}$ is the average permselectivity. The permselectivity expresses the capability of the membrane to transport a specific type of ion, either cation or anion.

The power requirement for an ED unit cell, excluding pumping power consumption, is:

$$P_{\mathrm{ED}}=E_{\mathrm{OCP}}i_{\mathrm{ED}}+R_{\Omega}i_{\mathrm{ED}}^2, \tag{11}$$

where $i$ is the current density (e.g. flux of charge) and $R_{\Omega}$ is the ohmic area resistance for a ED-RED unit cell, calculated as [41]:

$$R_{\Omega}=\frac{R_{\mathrm{AEM}}}{1-\beta}+\frac{R_{\mathrm{CEM}}}{1-\beta}+\frac{\rho_{\mathrm{c}}h_{\mathrm{c}}}{\epsilon^2}+\frac{\rho_{\mathrm{d}}h_{\mathrm{d}}}{\epsilon^2}, \tag{12}$$

where $R_{\mathrm{AEM}}$ and $R_{\mathrm{CEM}}$ are the area resistances of the AEM and CEM respectively and $\beta$ is the mask fraction or spacer shadow factor [8]. $h_{\mathrm{d}}$ and $h_{\mathrm{c}}$ are the heights of the dilute and concentrated solution channels, $\epsilon$ is the porosity (open area) of the spacer, where the spacers keep the CEM and AEM apart and enhance the mixing of the solutions [46]. $\rho_{\mathrm{c}}$ and $\rho_{\mathrm{d}}$ are the resistivity of the concentrated and dilute feed, respectively, given as:

$$\begin{aligned}&\rho_{\mathrm{sol},10}=a\cdot c^b\\&a=0.1476\pm0.0077\Omega\mathrm{m}\\&b=-0.959\pm0.013\Omega\mathrm{m},\end{aligned} \tag{13}$$

based on data from [47], where $\rho_{sol,10}$ is the solution resistivity at 10 °C (Ωm) and $c$ is the concentration (M) (the concentration is rewritten from ppm to M using [48]). The theoretical temperature effect on the resistivity is also obtained from [47]:

$$\rho_{\mathrm{sol}}=\rho_{\mathrm{sol},10}\frac{31.1\mathrm{K}}{T-251.5\mathrm{K}}, \tag{14}$$

where $T$ is the temperature in Kelvin. The reversible power density is given as:

$$P_{\mathrm{ED}}^{\mathrm{rev}}=i_{\mathrm{ED}}E_{\mathrm{OCP}}. \tag{15}$$

### 2.1.2. Discharging the electrodialytic storage system

Discharge of the electrodialytic energy storage system occurs through the (spontaneous) movement of ions from the concentrated to the dilute solution. The power density is expressed as:

$$P_{\mathrm{RED}}=E_{\mathrm{OCP}}i_{\mathrm{RED}}-R_{\Omega}i_{\mathrm{RED}}^2, \tag{16}$$

where $E_{\mathrm{OCP}}$ is obtained using Eq. (10). The current density corresponding to the peak power density of the discharging process is:

$$i_{\mathrm{RED}}^{\mathrm{peakpower}}=\frac{E_{\mathrm{OCP}}}{2R_{\Omega}}, \tag{17}$$

where the peak power density is:

$$P_{\mathrm{RED}}^{\mathrm{peak}}=\frac{E_{\mathrm{OCP}}^2}{4R_{\Omega}}. \tag{18}$$

It is worth mentioning that Eqs. (17) and (18) are valid if the stack and load resistances are equal [4,6].

### 2.1.3. Efficiencies for the electrodialytic energy storage system

Integration as of Eq. (6) gives the following charging efficiency:

$$\eta_{\mathrm{ED}}=\frac{W_{\mathrm{ED}}^{\mathrm{rev}}}{W_{\mathrm{pump}}+W_{\mathrm{ED}}} \tag{19}$$

Correspondingly, substituting $i_{\mathrm{ED}}=0.5\times i_{\mathrm{RED}}^{\mathrm{peakpower}}$ (following from the duck-curve) and neglecting pumping losses, the maximum efficiency of ED can be expressed as:

$$\eta_{\mathrm{ED}}^{\mathrm{max}}=\frac{i_{\mathrm{ED}}E_{\mathrm{OCP}}}{E_{\mathrm{OCP}}i_{\mathrm{ED}}+R_{\Omega}i_{\mathrm{ED}}^2}=\frac{E_{\mathrm{OCP}}^2/4R_{\Omega}}{E_{\mathrm{OCP}}^2/4R_{\Omega}+E_{\mathrm{OCP}}^2/16R_{\Omega}}=\frac{4}{5} \tag{20}$$

The efficiency of the discharging process is given as:

$$\eta_{\mathrm{RED}}=\frac{W_{\mathrm{RED}}^{\mathrm{peak}}-W_{\mathrm{pump}}}{W_{\mathrm{RED}}^{\mathrm{rev}}}, \tag{21}$$

expressing the ratio of the net energy generated by RED and the (potential) chemical energy between two solutions. Neglecting the pumping losses, the efficiency can be expressed as:

$$\eta_{\mathrm{RED}}^{\mathrm{max}}=\frac{E_{\mathrm{OCP}}^2/4R_{\Omega}}{E_{\mathrm{OCP}}^2/2R_{\Omega}}=\frac{1}{2}, \tag{22}$$

i.e., the maximum efficiency of RED is 0.5, considering the proposed definition of efficiency [6].

The round-trip efficiency of the electrodialytic energy storage system is:

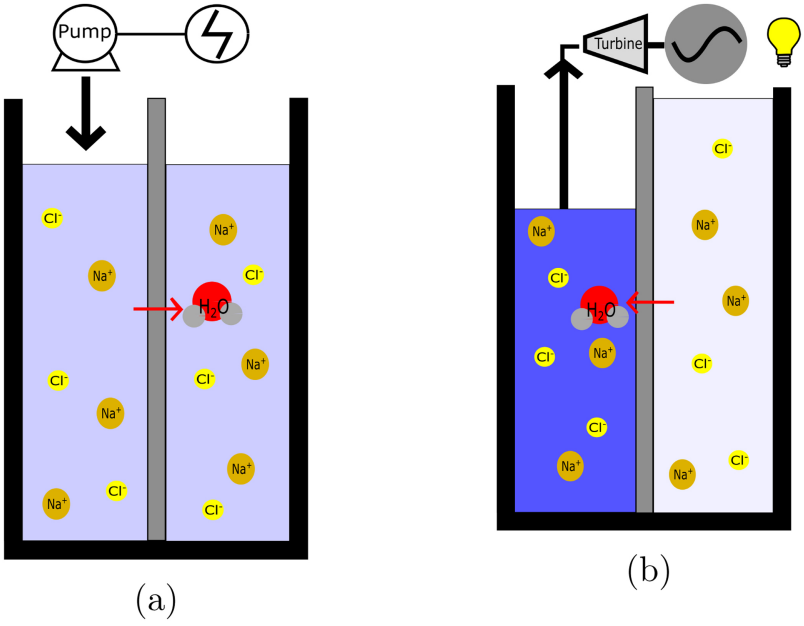


**Fig. 5.** The figure shows a schematic of the osmotic energy storage system. (a) During charging by RO, ions concentration is increased in one solution compared to the other solution due to water movement from high salinity solution towards to low salinity solution. (b) During discharging by PRO, the water flux is reversed, and water moves back from the dilute to concentrated solution, eventually re-establishing the initial condition. Further details of RO-PRO with pressure exchanger (PX) and all flow streams can be found in [13,51].

$$\eta_{\mathrm{ED-RED}} = \eta_{\mathrm{ED}}\eta_{\mathrm{RED}} = \left(\frac{W_{\mathrm{RED}}^{\mathrm{peak}} - W_{\mathrm{pump}}}{W_{\mathrm{ED}} + W_{\mathrm{pump}}}\right)\left(\frac{i_{\mathrm{ED}}}{i_{\mathrm{RED}}}\right), \tag{23}$$

which, as of Eqs. (20) and (22) has a maximum efficiency of 0.4.

### 2.2. Osmotic energy storage system; RO-PRO

Reverse osmosis is a separation method using semipermeable membranes, where water is transported through the membrane when a pressure exceeding the osmotic pressure is applied. The technology was developed in the late sixties for desalination [49,12].

An operating pressure around 30–80 bar is typically used for a conversion system of seawater to freshwater utilising commercial membranes [49]. In RO, water is transported through the membrane; thus, demineralised water is accumulated in one side of the membrane and impurities are left in the other side.

Pressure retarded osmosis is the opposite process of RO [2,50]. Water diffuses through the membrane from a low salinity solution to a high salinity solution due to the driving force of the chemical potential gradient across the membrane. An illustration of the osmotic energy storage system is shown in Fig. 5.

Reverse osmosis applies hydrostatic pressure as the driving force for separation, which has to counteract the osmotic pressure that would otherwise favour water flux from the dilute to the concentrated solution. Accordingly, in RO, there is a need for a high-pressure pump and high-pressure vessel to provide a level of energy that can overcome natural osmotic pressure; typically 20–25 bar between the fresh water and seawater [2]. The efficiency can be increased by implementing pressure exchangers (PX) which transfer energy from the high-pressure stream to a low-pressure stream. In the RO-PRO energy storage system, the low-pressure feed stream into RO (high salinity) can be pressurised by the high-pressure draw stream exiting from PRO, reducing the required energy by up to 60% [13,51].

The power needed for pumping water through the two channels in the RO-PRO system is considered to be the same for both channels. This simplification underestimates the power required because the flow velocity is different in the two channels. Consider for example the flow at the end of the membrane in a PRO module; because 70–80% of the feed solution ends up in the draw solution, the flow rate at the outlet becomes 7 times larger on the salty side than on the water side (1.75/0.25 = 7). Because pumping power is proportional to the square of the velocity, the pumping power in the end region of the draw side becomes 3 times ($1.75^2$) higher at the outlet than at the inlet. Even if the pumping power at the outlet of the waterside lowers to 0.06 ($0.25^2$) of the inlet need, the total pumping power needs increases by up to 50% compared to the simplified assessment in this study. Because of the non-linearity of this type of calculation, we consider the selected simplification to be sufficient. We find this because the pumping power is typically less than 10% [3] of the system power output so that the net power output only varies with a few percentages (up to 5%).

#### 2.2.1. Charging the osmotic energy storage system

The charging step of the proposed energy storage system is performed by RO. The pressure difference between the two solutions acts as the driving force for this process and is defined as [4]:

$$\mathcal{E}_{\mathrm{RO/PRO}}^{\mathrm{drive}} = \Delta\pi = 2\mathrm{RT}(c_{\mathrm{c}} - c_{\mathrm{d}}), \tag{24}$$

where $\Delta\pi$ is the osmotic pressure, $c_{\mathrm{c}}$ and $c_{\mathrm{d}}$ are the concentration of concentrated and the dilute solutions respectively (with unit mol/$\mathrm{m}^3$, equal to 1000 M), $R$ is universal gas constant and $T$ is temperature.

The hydrostatic pressure for RO can be calculated by:

$$\Delta P_{\mathrm{h}} = \Delta\pi + \frac{J_{\mathrm{RO}}}{K_{\mathrm{w}}}, \tag{25}$$

and the corresponding power density is:

$$P_{\mathrm{RO}} = J_{\mathrm{RO}}\Delta P_{\mathrm{h}} = \Delta\pi J_{\mathrm{RO}} + \frac{J_{\mathrm{RO}}^2}{K_{\mathrm{w}}}, \tag{26}$$

where $J_{\mathrm{RO}}$ is the water flux and $K_{\mathrm{w}}$ is the permeability of the membrane with respect to water. The reversible power density is:

$$P_{\mathrm{RO}}^{\mathrm{rev}} = \Delta\pi J_{\mathrm{RO}} \tag{27}$$

It should be noted that the water flux is normally expressed as a function of hydrostatic and osmotic pressure, cf. [4,2,3,50], however, to keep an analogy to ED-RED and MCDI-CDP the reverse relation is used in the current work.

#### 2.2.2. Discharging the osmotic energy storage system

Discharging the osmotic energy storage system occurs when water from the low salinity solution diffuses to the high salinity solution. Contrary to RO, PRO is a low-pressure process. In PRO, the applied hydrostatic pressure, which is needed to pressurise the high salinity solution, is described by Eq. (28) [4]:

$$\Delta P_{\mathrm{h}} = \Delta\pi - \frac{J_{\mathrm{PRO}}}{K_{\mathrm{w}}} \tag{28}$$

The power density of PRO is the product of water flux across the membrane and the hydrostatic pressure drop according to Eq. (29):

$$P_{\mathrm{PRO}} = J_{\mathrm{PRO}}\Delta P_{\mathrm{h}} = \Delta\pi J_{\mathrm{PRO}} - \frac{J_{\mathrm{PRO}}^2}{K_{\mathrm{w}}} \tag{29}$$

The peak power density is obtained when the water flux is defined as Eq. (30):

$$J_{\mathrm{PRO}}^{\mathrm{peakpower}} = \frac{K_{\mathrm{w}}}{2}\Delta\pi, \tag{30}$$

analogous to Eq. (17) when determining the current density in RED.

The corresponding peak power density is given as [4]:

$$P_{\mathrm{PRO}}^{\mathrm{peak}} = \frac{K_{\mathrm{w}}}{4}\Delta\pi^2, \tag{31}$$

while the reversible power density is defined as:

$$P_{\mathrm{PRO}}^{\mathrm{rev}} = \Delta\pi J_{\mathrm{PRO}} \tag{32}$$

#### 2.2.3. Efficiencies for the osmotic energy storage system

Following the definitions introduced earlier, the efficiency for PRO is given as:

$$\eta_{\mathrm{PRO}} = \frac{(W_{\mathrm{PRO}}^{\mathrm{peak}} - W_{\mathrm{pump}})}{W_{\mathrm{PRO}}^{\mathrm{rev}}}, \tag{33}$$

again expressing the ratio of (the net) energy generated by PRO and the (potential) chemical energy between two solutions. Neglecting the pumping losses, the maximum efficiency can be expressed as:

$$\eta_{\mathrm{PRO}}^{\mathrm{max}} = \frac{K_w\Delta\pi^2/4}{K_w\Delta\pi^2/2} = \frac{1}{2}, \tag{34}$$

corresponding to that found for RED.

The efficiency of RO is expressed as:

$$\eta_{\mathrm{RO}} = \frac{W_{\mathrm{RO}}^{\mathrm{rev}}}{(W_{\mathrm{pump}} + W_{\mathrm{RO}})}. \tag{35}$$

Substituting $J_{\mathrm{RO}} = 0.5 \times J_{\mathrm{PRO}}^{\mathrm{peakpower}}$ and neglecting pumping losses, the efficiency of RO under the prescribed conditions is:

$$\eta_{\mathrm{RO}} = \frac{J_{\mathrm{RO}}\Delta\pi}{J_{\mathrm{RO}}\Delta\pi + J_{\mathrm{RO}}^2/K_w} = \frac{K_w\Delta\pi^2/4}{K_w\Delta\pi^2/4 + K_w\Delta\pi^2/16} = \frac{4}{5} \tag{36}$$

The efficiency of the osmotic energy storage system ($\eta_{RO-PRO}$) can be defined as Eq. (37) as a measure of the fraction of the power densities by discharging and charging.

$$\eta_{\mathrm{RO-PRO}} = \left(\frac{W_{\mathrm{PRO}}^{\mathrm{peak}} - W_{\mathrm{pump}}}{W_{\mathrm{RO}} + W_{\mathrm{pump}}}\right)\left(\frac{J_{\mathrm{RO}}}{J_{\mathrm{PRO}}}\right), \tag{37}$$

again limited to maximum efficiency of 0.4 at when following the duck-curve constraint and peak-power discharge water flux.

### 2.3. Capacitive energy storage system; MCDI-CDP

A third technique to store energy via salinity gradients can be realised by combining MCDI and CDP. During both charging and discharging, ions enter and leave the porous electrodes [52–54]. Consequently, the capacitance of the system is playing an essential role in the performance of this energy storage system.

#### 2.3.1. Charging the capacitive energy storage system

The charging of the system is based on MCDI, first introduced by Claude et al. [55,56], as illustrated in Fig. 6. An AEM and a CEM are placed on each electrode, enabling selective ion transport.

Membrane capacitive deionisation consists of four steps. In the first step, a mixed solution flows between two membrane-covered electrodes at open circuit. During the second step, a potential is applied over the electrodes, making the positive ions flow to the negative electrode and vice versa, forming an electrical double layer [57,56] and a Donnan potential, where the outlet solution is less concentrated than the inlet. In the third step, the outer circuit is opened again, letting some ions travel from the electrodes to the solution. During the fourth step the potential is reversed compared to the second step, and the ions are forced from the electrodes to the solution. The outlet solution from the system is now more concentrated than the inlet and is led to a new compartment.

During addition and removal of ions, step 2 and step 4, the time-dependent capacitive potential gradually reduces the drive potential.

#### 2.3.2. Discharging the capacitive energy storage system

Capacitive Donnan potential was first proposed by Sales et al. in 2010 [58] and can be realised with a cell design corresponding to MCDI [59]. An illustration of a CDP system with the ionic flow is shown in Fig. 7.

The CDP process consists of four steps. In the first step, the membrane-covered electrodes are polarised by immersing them in a concentrated solution at open circuit, resulting in a Donnan potential at each electrode. In the second step, the electrodes are connected to an external load allowing a flow of an electric current in an outer circuit, until electrodes attain charge neutrality. In the third step, the circuit is open again, and the concentrated solution is replaced by a dilute solution. The concentration in the electrodes is now higher than the concentration in the solution, promoting ion transport to the solution due to the reversed Donnan potential [60]. In the last step, the electrodes are connected to an external load again, where the electrons flow in the opposite direction compared to the second step.

#### 2.3.3. Potential from CDP and MCDI

The model of the capacitive energy storage system takes the second and fourth step into account, while excluding the two steps in which the solution in the cell is changed. The driving force is the sum of the Donnan-, $E_{\mathrm{Donnan}}$, and capacitive potential, $E_{\mathrm{c}}$, i.e.

$$\mathcal{E}_{\mathrm{MCDI/CDP}}^{\mathrm{drive}} = E_{\mathrm{Donnan}} + E_{\mathrm{c}}, \tag{38}$$

while the cell potential is expressed as [25]:

$$E_{\mathrm{MCDI/CDP}} = E_{\mathrm{Donnan}} + E_{\mathrm{c}} - \mathrm{i}R_{\Omega}, \tag{39}$$

where $i$ is the current density, defined as positive when adding ions to the electrode and negative when ions are removed, and $R_{\Omega}$ is the ohmic resistance. The Donnan potential is calculated as:

$$E_{\mathrm{Donnan}} = 2\tilde{\alpha}\frac{\mathrm{RT}}{\mathrm{zF}}\ln\left(\frac{c_{\mathrm{sp}}}{c_{\mathrm{el}}}\right), \tag{40}$$

differing slightly from the Nernst equation (Eq. (10)), due to the specification of the concentration in the spacer, $c_{\mathrm{sp}}$, and electrode, $c_{\mathrm{el}}$. The potential in MCDI and CDP alternates between positive and negative depending on whether the concentration is highest in the spacer or in the electrode [59,61]. The capacitive potential for CDP and MCDI is given in Eqs. (41) and (42), respectively:

$$E_{\mathrm{c,CDP}} = E_{\mathrm{c},0} - \frac{i_{\mathrm{CDP}}}{C_{\mathrm{CDP}}}t_{\mathrm{CDP}} \tag{41}$$

$$E_{\mathrm{c,MCDI}} = E_{\mathrm{c},0} + \frac{i_{\mathrm{MCDI}}}{C_{\mathrm{MCDI}}}t_{\mathrm{MCDI}}, \tag{42}$$

where $E_{\mathrm{c},0}$ is the initial capacitive potential at the start of a new step in the cycle, $C$ is the capacitance of the unit cell and $t_{\mathrm{MCDI}}$ and $t_{\mathrm{CDP}}$ is the time between a new concentration entering the cell, until the total potential reaches zero, i.e.:

$$t_{\mathrm{MCDI}} = \frac{C}{i}(-E_{\mathrm{d}} - E_{\mathrm{c},0} + \mathrm{i}R_{\Omega}) \tag{43}$$

$$t_{\mathrm{CDP}} = \frac{C}{i}(E_{\mathrm{d}} + E_{\mathrm{c},0} - \mathrm{i}R_{\Omega}) \tag{44}$$

When adding ions to the electrodes in CDP and removing ions from the electrodes in MCDI, the solution in the spacer is concentrated. The resistance is in this case given as:

$$R_{\Omega,\mathrm{CDP}}^{\mathrm{add}} = R_{\Omega,\mathrm{MCDI}}^{\mathrm{remove}} = \frac{R_{\mathrm{AEM}}}{1-\beta} + \frac{R_{\mathrm{CEM}}}{1-\beta} + \frac{\rho_{\mathrm{c}}h_{\mathrm{c}}}{\epsilon^2} + R_{\mathrm{electrodes}} \tag{45}$$

Correspondingly, while both removing ions from the electrodes in CDP and adding ions to the electrodes in MCDI, the solution in the spacer is

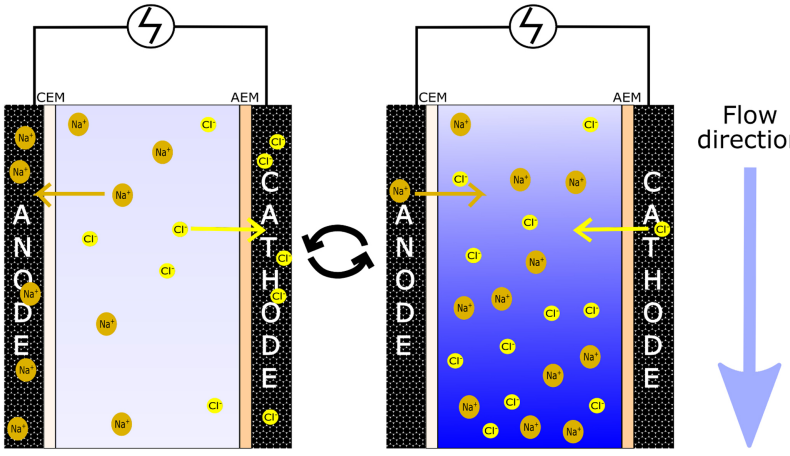


**Fig. 6.** The figure shows an illustration of the MCDI technology. A solution flows into the system which alternates between producing a diluted (left) and concentrated solution (right) by alternating ion exchange with porous electrodes. Electrodes are charged when producing the dilute solution and discharged when producing the concentrated solution. Each solution is stored in separate containers.

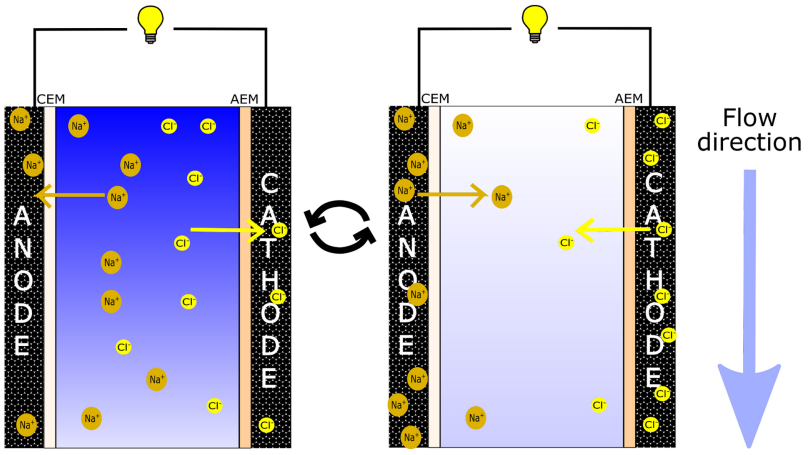


**Fig. 7.** The figure shows an illustration of the CDP technology. Concentrated (left) and dilute (right) solutions flow alternately into the system producing a solution of mixed concentration. Electrodes are charged while the concentrated solution is flowing and discharged to the dilute solution in a spontaneous (energy producing) process.

dilute, with resistance equal to:

$$R_{\Omega,\mathrm{CDP}}^{\mathrm{remove}} = R_{\Omega,\mathrm{MCDI}}^{\mathrm{add}} = \frac{R_{\mathrm{AEM}}}{1-\beta} + \frac{R_{\mathrm{CEM}}}{1-\beta} + \frac{\rho_{\mathrm{d}} h_{\mathrm{d}}}{\epsilon^2} + R_{\mathrm{electrodes}} \tag{46}$$

In Eqs. (45) and (46), $R_{\mathrm{AEM}}$ and $R_{\mathrm{CEM}}$ are the area resistances of the AEM and CEM respectively, $\beta$ is the shadow factor of the spacer, $h_{\mathrm{c}}$ and $h_{\mathrm{d}}$ are the heights of the concentrated and dilute compartment respectively, $\epsilon$ is the porosity of the spacer and $\rho_{\mathrm{c}}$ and $\rho_{\mathrm{d}}$ is the resistivity of the concentrated and dilute solution respectively (Eqs. (13) and (14)).

By substitution, the potential adding and removing ions to and from the electrodes for CDP and MCDI is:

$$E_{\mathrm{CDP}}^{\mathrm{add}} = 2\bar{\alpha}\frac{\mathrm{RT}}{F}\ln\left(\frac{c_{\mathrm{sp}}}{c_{\mathrm{el}}}\right) + E_{\mathrm{c},0} - \frac{i}{C}t - i\left(\frac{R_{\mathrm{AEM}}}{1-\beta} + \frac{R_{\mathrm{CEM}}}{1-\beta} + \frac{\rho_{\mathrm{c}} h_{\mathrm{c}}}{\epsilon^2}\right) \tag{47}$$

$$E_{\mathrm{CDP}}^{\mathrm{remove}} = 2\bar{\alpha}\frac{\mathrm{RT}}{F}\ln\left(\frac{c_{\mathrm{sp}}}{c_{\mathrm{el}}}\right) + E_{\mathrm{c},0} - \frac{i}{C}t - i\left(\frac{R_{\mathrm{AEM}}}{1-\beta} + \frac{R_{\mathrm{CEM}}}{1-\beta} + \frac{\rho_{\mathrm{d}} h_{\mathrm{d}}}{\epsilon^2}\right) \tag{48}$$

$$E_{\mathrm{MCDI}}^{\mathrm{add}} = 2\bar{\alpha}\frac{\mathrm{RT}}{F}\ln\left(\frac{c_{\mathrm{sp}}}{c_{\mathrm{el}}}\right) + E_{\mathrm{c},0} + \frac{i}{C}t - i\left(\frac{R_{\mathrm{AEM}}}{1-\beta} + \frac{R_{\mathrm{CEM}}}{1-\beta} + \frac{\rho_{\mathrm{d}} h_{\mathrm{d}}}{\epsilon^2}\right) \tag{49}$$

$$E_{\mathrm{MCDI}}^{\mathrm{remove}} = 2\bar{\alpha}\frac{\mathrm{RT}}{F}\ln\left(\frac{c_{\mathrm{sp}}}{c_{\mathrm{el}}}\right) + E_{\mathrm{c},0} + \frac{i}{C}t - i\left(\frac{R_{\mathrm{AEM}}}{1-\beta} + \frac{R_{\mathrm{CEM}}}{1-\beta} + \frac{\rho_{\mathrm{c}} h_{\mathrm{c}}}{\epsilon^2}\right). \tag{50}$$

Fig. 8 shows the potential with respect to the time, given constant current for two cycles for CDP and MCDI. The solutions are switched when the total potential is zero, and the model is run until the change in initial capacitive potential is less than 0.1%.

### 2.3.4. Current density in the capacitive energy storage system

The current density for adding and removing ions to and from the electrodes in CDP, is chosen at maximum power density, given in Eqs. (51) and (52):

$$i_{\mathrm{CDP}}^{\mathrm{add}} = \frac{E_{\mathrm{Donnan}} + E_{\mathrm{c},0}}{2t^{\mathrm{add}}/C^{\mathrm{add}} + 2R_{\Omega,\mathrm{CDP}}^{\mathrm{add}}}, \tag{51}$$

$$i_{\mathrm{CDP}}^{\mathrm{remove}} = \frac{E_{\mathrm{Donnan}} + E_{\mathrm{c},0}}{2t^{\mathrm{remove}}/C^{\mathrm{remove}} + 2R_{\Omega,\mathrm{CDP}}^{\mathrm{remove}}}, \tag{52}$$

Since a fixed current density and water flux is used in the modelling of ED-RED and RO-PRO, corresponding conditions are assumed for MCDI-CDP for the sake of comparison. The maximum power- and corresponding current density is determined graphically from plots generated by varying $t^{\mathrm{add}}$ and $t^{\mathrm{remove}}$ in Eqs. (51) and (52). An example of power density as a function of current density at 25 °C for 30 different concentrations between 0 and 1 M is given in Fig. 9.

The discharging current is half of the charging current and visa verse, corresponding to the systems described previously:

$$i_{\mathrm{MCDI}}^{\mathrm{add}} = -\frac{i_{\mathrm{CDP}}^{\mathrm{remove}}}{2} \tag{53}$$

$$i_{\mathrm{MCDI}}^{\mathrm{remove}} = -\frac{i_{\mathrm{CDP}}^{\mathrm{add}}}{2} \tag{54}$$

### 2.3.5. Power and energy density from CDP and MCDI

The average power density, while adding and removing ions from the electrodes in both CDP and MCDI is:

$$\bar{P} = \frac{1}{\Delta t}\int_{t_1}^{t_2} \mathrm{P}\,\mathrm{dt} = \frac{1}{\Delta t^{\mathrm{add}} + \Delta t^{\mathrm{remove}}}\left(\int_{t_1^{\mathrm{add}}}^{t_2^{\mathrm{add}}} P^{\mathrm{add}}\mathrm{dt} + \int_{t_1^{\mathrm{remove}}}^{t_2^{\mathrm{remove}}} P^{\mathrm{remove}}\mathrm{dt}\right), \tag{55}$$

where $\Delta t^{\mathrm{add}} = {t_2}^{\mathrm{add}} - {t_1}^{\mathrm{add}}$ and $\Delta t^{\mathrm{remove}} = {t_2}^{\mathrm{remove}} - {t_1}^{\mathrm{remove}}$ are the

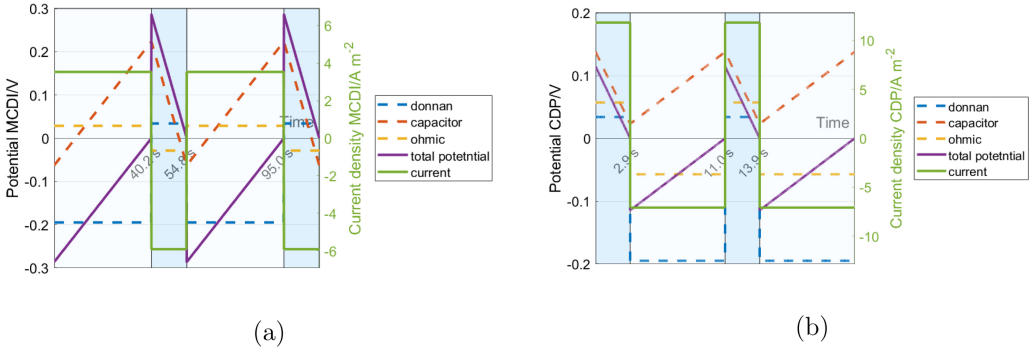


**Fig. 8.** Potential with respect to the time in MCDI (a) and CDP (b) for two cycles. Light colour indicates a dilute solution, where ions are added to the electrodes for MCDI and removed in CDP. Dark colour indicates a concentrated solution, where ions are removed from the electrodes for MCDI and added for CDP. (For interpretation of the references to colour in this figure legend, the reader is referred to the web version of this article.)

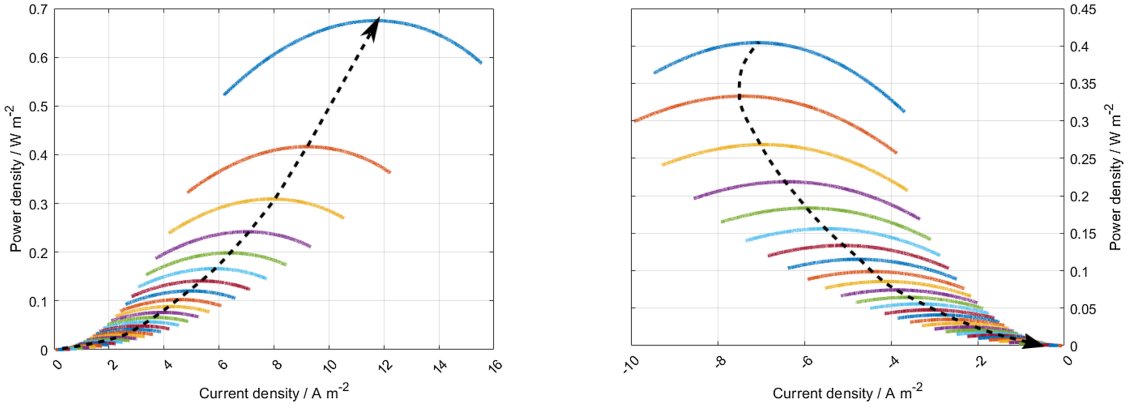


**Fig. 9.** Power density as a function of current density for CDP while adding ions to the electrodes (a) and removing the ions from the electrode (b). The black dotted lines give the maximum power density, where the arrow indicates direction of increasing concentration. The temperature is 25 °C.

time which take to add and remove ions from the electrode respectively.

The reversible power density from one cycle of CDP and MCDI is the product of the current density and the drive potential, where the latter is the summation of Donnan potential (Eq. (40)) and the capacitive potential (Eq. (41)).

$$\bar{P}_j^{\text{rev}} = \frac{1}{\Delta t}\int_{t_1}^{t_2} i_j(E_{\text{Donnan}} + E_c)\text{d}t \tag{56}$$

### 2.4. Efficiency of CDP and MCDI

Corresponding to the other technologies, the relevant efficiencies are given as:

$$\eta_{\text{CDP}} = \frac{W_{\text{CDP}}^{\text{peak}} - W_{\text{pump}}}{W_{\text{CDP}}^{\text{rev}}}, \tag{57}$$

$$\eta_{\text{MCDI}} = \frac{W_{\text{MCDI}}^{\text{rev}}}{W_{\text{MCDI}} + W_{\text{pump}}} \tag{58}$$

and

$$\eta_{\text{MCDI-CDP}} = \eta_{\text{MCDI}}\eta_{\text{CDP}} = \frac{W_{\text{CDP}}^{\text{peak}} - W_{\text{pump}}}{W_{\text{CDP}}^{\text{rev}}}\frac{W_{\text{MCDI}}^{\text{rev}}}{W_{\text{MCDI}} + W_{\text{pump}}} \tag{59}$$

Neglecting the pumping losses, the maximum efficiency can be found to be equivalent to the other technologies, i.e. 0.5 for CDP, 0.8 for MCDI and 0.4 for the round-trip efficiency.

## 3. Results and discussion

The following section describes the results for each energy storage system separately, where each subsection contains drive potential, power density and efficiency of the charging and discharging, in addition to the total efficiency. The maximum power density with respect to concentrations is also calculated for each discharging process for temperature varying from 10 °C to 80 °C. Finally, the average electricity price in USA and EU is compared to the cost of all three energy storage system, given different membrane prices. The input parameters for the three models are given in Table 1.

### 3.1. Electrodialytic energy storage; ED-RED

The open circuit potential with respect to the concentration of dilute solution at different temperatures is demonstrated in Fig. 10, while the ohmic resistance over one unit cell is plotted in Fig. A.25(a) in Appendix A. The main contributor to the resistance is the resistivity of the dilute solution. The peak power current density to discharge the electrodialytic energy storage system, is depicted in Fig. A.25(b) in Appendix A.

The peak power current density (Eq. (17)) is proportional to the open circuit potential, and inversely proportional to the resistance. As the resistance is increasing faster than the open circuit potential at low concentrations, the overall effect is a reduction in the peak power current densities at these concentrations, as shown in Fig. A.25(b).

The power density of charging and discharging of electrodialytic

**Table 1**
Input values used for models of the three energy storage systems. A discussion regarding additional parameters is given in Appendix D.

| Name | Symbol | Value |
|---|---|---|
| Channel height | $h$ | $2 \times 10^{-4}$ m [41] |
| Channel length | $l$ | 0.1 m [41] |
| Channel width | $w$ | 0.1 m [41] |
| Porosity spacer | $\epsilon$ | 0.7 [41] |
| Open area spacer | $\sigma$ | 0.5 [41] |
| Ratio surface to volume spacer filament | $S_{\text{sp}}/V_{\text{sp}}$ | 8/h |
| Hydraulic diameter | $D_{\text{h}}$ | See Eq. (5) |
| Power losses pump | $P_{\text{pump}}$ | See Eq. (3) |
| Mean permselectivity CEM and AEM | $\bar{\alpha}$ | 0.97 [62–64] |
| Resistance AEM | $r_{\text{AEM}}$ | $1.0 \times 10^{-4}\,\Omega\,\text{m}^2$ [62,63] |
| Resistance CEM | $r_{\text{CEM}}$ | $1.0 \times 10^{-4}\,\Omega\,\text{m}^2$ [62,64] |
| Concentration, concentrated solution | $c_c$ ($c_c = 1 - c_d$) | 0.99–0.51 M |
| Concentration, dilute solution | $c_d$ | 0.01–0.49 M |
| Conc. porous electrodes (MCDI & CDP) | $c_m$ | 0.5 M |
| Temperature | $T$ | [283 298 313 333 353] K |
| Viscosity solution | $\mu$ | Eq. (4) |
| Solution resistivity | $\rho_{c/d}$ | Eqs. (13) and (14) |
| Water permeability in membrane | $K_w$ | $4.1 \times 10^{-13}\,\text{m}\,(\text{Pa s})^{-1}$ [4] |
| Residence times | $t_{\text{res}}$ | [10 20 40 70 100] s [41][a] |
| Corresponding velocities based on $l/t_{res}$ | $\bar{u}$ | [10 5.0 2.5 1.4 1.0] mm/s |
| Capacitance (CDP &MCDI) | C | $4 \times 10^{-2}\,\text{F m}^{-2}$ [61] |
| Resistance electrodes (MCDI & CDP) | $R_e$ | $4.4 \times 10^{-3}\,\Omega\,\text{m}^2$ [65] |
| Molar mass NaCl | $M$ | $58.44\,\text{mol g}^{-1}$ |
| Faraday's constant | $F$ | $96{,}485\,\text{C mol}^{-1}$ |
| Universal gas constant | $R$ | $8.314\,\text{J K}^{-1}\,\text{mol}^{-1}$ |

[a] Vermaas et al. [41] considered residence times from 0.5 to 200 s to calculate power density from salinity gradient using RED, demonstrating that both too high and too low values were detrimental for system performance.

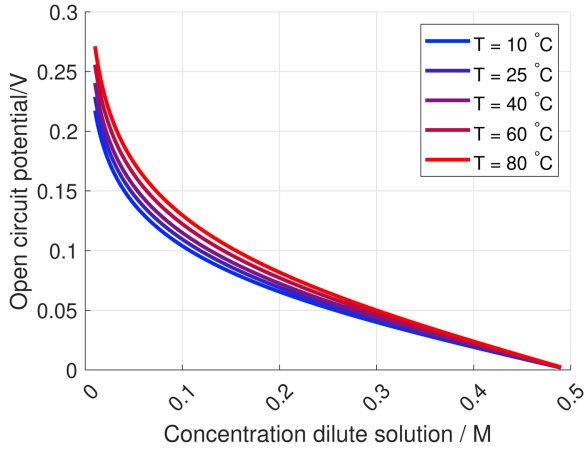


**Fig. 10.** Open circuit potential for one unit cell of RED and ED. $c_c = 1 - c_d$.

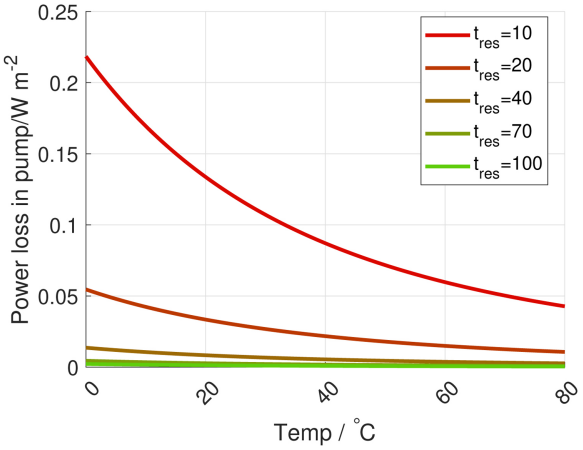


**Fig. 12.** This figure shows the pumping loss per unit cell area in electrodialytic and osmotic energy storage systems at different temperatures at $C_d = 0.25$ M and $C_c = 0.75$ M.

energy storage system, is presented in Fig. 11. The maximum power density is at a dilute concentration between 0.046 and 0.026 M, where the RED power density is changing from 3.18 to 11.0 W m$^{-2}$, corresponding to temperatures from 10 °C to 80 °C. The power density at lower dilute concentration is more affected by the drop in current density due to resistance, than the increase in the open circuit potential. The reduction in power density with decreased dilute concentration is in agreement with the theoretical and experimental research by Egmond et al. [19].

The pumping loss as a function of concentration changes less than 0.2% over the total concentration range at fixed temperature and residence time. The pumping loss is plotted as a function of residence time, i.e. the time the fluid spends from inlet to outlet, and temperature in Fig. 12. At lower residence time the influence of temperature on the pump power consumption is greater than at higher residence time. However, at lower temperatures, the influence of residence time is more notable than at higher temperatures. The pumping power loss is reduced by a factor of 100 when increasing the residence time by a factor of 10; from 10 s to 100 s, corresponding to a decrease in velocity of factor 10. Changing the temperature from 10 °C to 80 °C, lowers the pumping loss with a factor 25.

The efficiency of charging and discharging the electrodialytic energy storage system at different residence times is displayed in Fig. 13(a) and (b), while the total efficiency is shown in Fig. 13(c) for a fixed temperature, $T = 25$ °C.

At the beginning of the discharge process, due to the high concentration difference between the two streams, the energy storage system has a high efficiency where the power generation is higher than the pump power consumption. The efficiency is decreasing as the concentration difference decreases, due to relatively higher energy consumed by the pumps compared to the energy produced. The efficiencies for ED and RED with respect to temperature are given in Fig. 14(a) and (c), respectively. The total electrodialytic energy storage system efficiency, is given in Fig. 14, considering a constant residence time equal to 20 s. The efficiency in RED and ED increases by elevating temperature, due to temperature dependency on drive potential, resistance and pumping losses.

### 3.2. Osmotic energy storage; RO-PRO

The osmotic pressure difference, $\Delta\pi$, for different temperatures is demonstrated in Fig. 15, while the corresponding water flux for peak power density is shown in Fig. A.26 in Appendix A.

The power densities produced from PRO and consumed in RO are given in Fig. 16. The maximum power density for PRO is changing from 4.36 to 6.78 W m$^{-2}$ corresponding to temperatures from 10 °C to 80 °C, while the pumping losses are the same as for the electrodialytic energy storage system (see Fig. 12).

The efficiency of charging and discharging for different residence times, with respect to the dilute concentration and constant temperature, $T = 25$ °C, is shown in Fig. 17(a) and (b). The total efficiency is given in Fig. 17(c). The efficiencies of PRO and RO are enhanced by

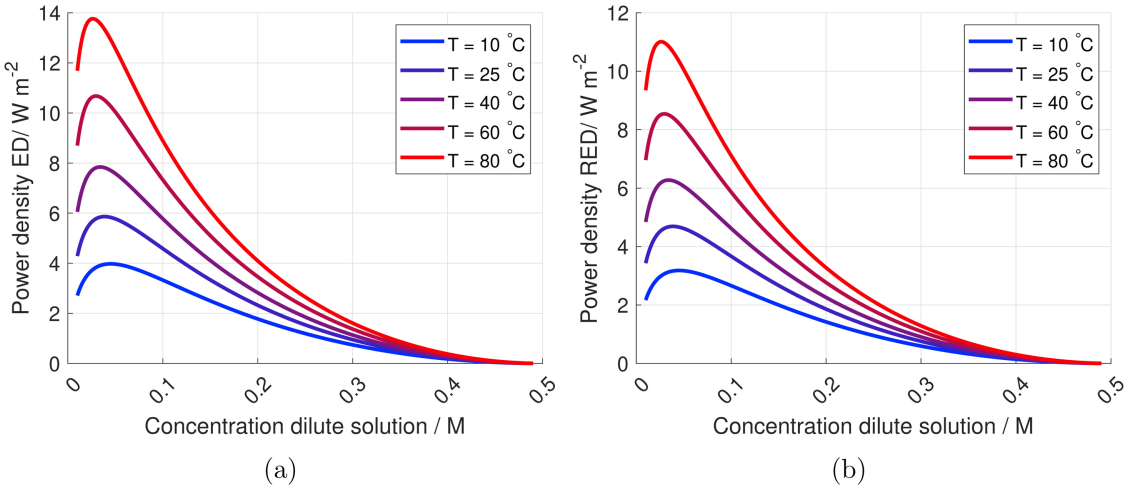


**Fig. 11.** Power per unit cell area while charging (a) and discharging (b) the electrodialytic energy storage system. $c_c = 1 - c_d$.

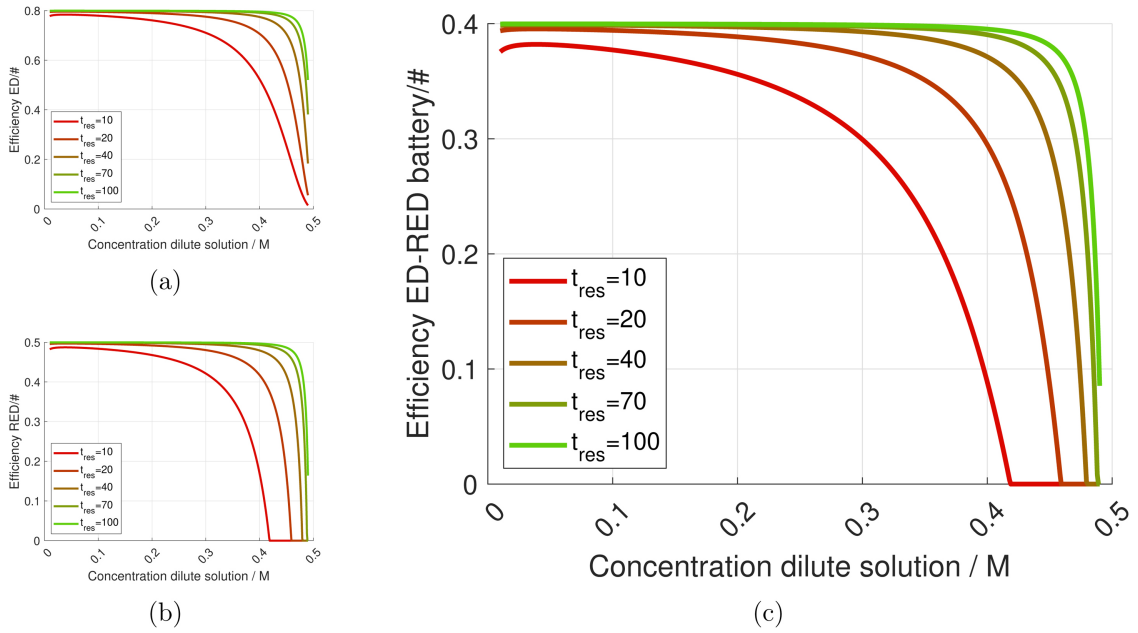


**Fig. 13.** Efficiency at different residence times for (a) ED, (b) RED and (c) total electrodialytic energy storage system at T = 25 °C and $c_c = 1 - c_d$.

increased residence time, due to the decreasing in pumping losses.

The efficiencies of RO and PRO for different temperatures at fixed residence time, $t_{res} = 20$ s, is shown in Fig. 18(a) and (b), where the total efficiency of osmotic energy storage system is given in Fig. 18(c). The efficiency for PRO and RO increases by elevating temperature, due to the temperature dependency of viscosity and osmotic pressure.

Similarly to the efficiency of the ED-RED energy storage system in Fig. 14, the efficiency of osmotic energy storage system decreases as the concentration difference decreases. The efficiency of the energy storage system is dominated by the PRO process at the early stage of the curve, while the RO energy consumption is controlling the late stage of the curve. Also, as the energy consumption by pump increases (i.e. residence time decreases), the efficiency of osmotic energy storage system decreases at a constant concentration of the dilute solution.

### 3.3. Membrane capacitive energy storage system; MCDI-CDP

The mean drive potential with respect to time in the membrane capacitive energy storage system is presented in Fig. 19, while the ohmic resistance of a unit cell is presented in Fig. A.27(a) (Appendix A) at different temperatures. The ohmic resistance is higher in the membrane capacitive energy storage system compared to the electrodialytic energy storage system due to the resistance of the porous electrodes included in every unit cell.

Depending on the concentration in the spacer and the state of charge, the current at peak power density changes. The current density decreases at lower concentrations, due to an increased cell resistance. The average power densities gained from CDP and the average consumed power density in MCDI are shown in Fig. 20. The power density obtained from CDP is 0.8 of what is consumed by MCDI.

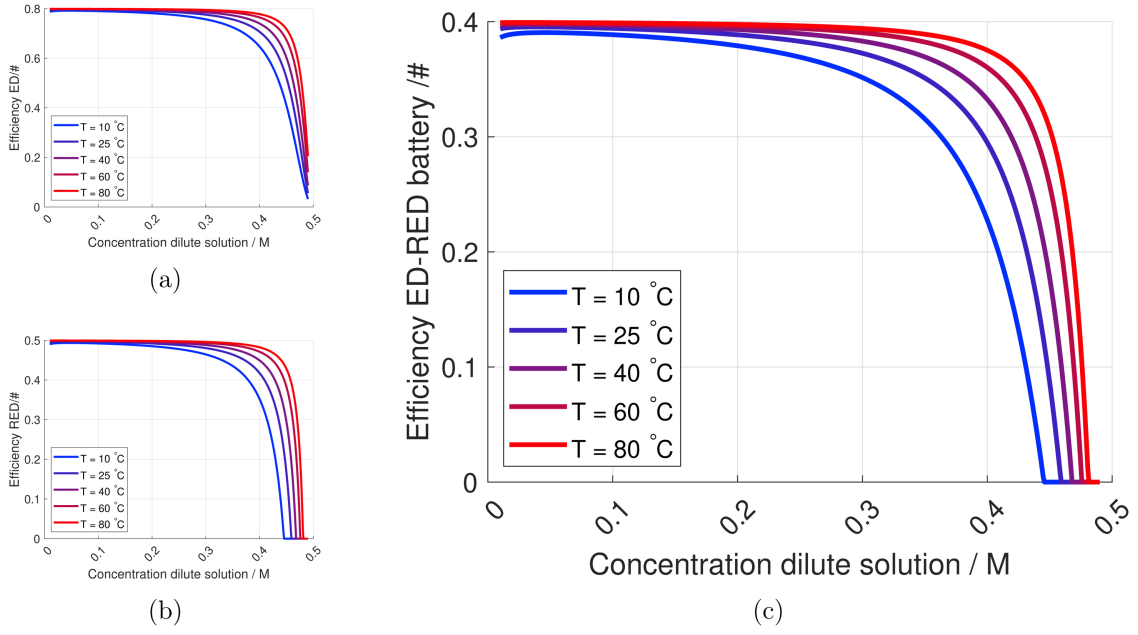


**Fig. 14.** Efficiency at different temperatures for (a) ED and (b) RED and (c) total electrodialytic energy storage system. $t_{res} = 20$ s and $c_c = 1 - c_d$.

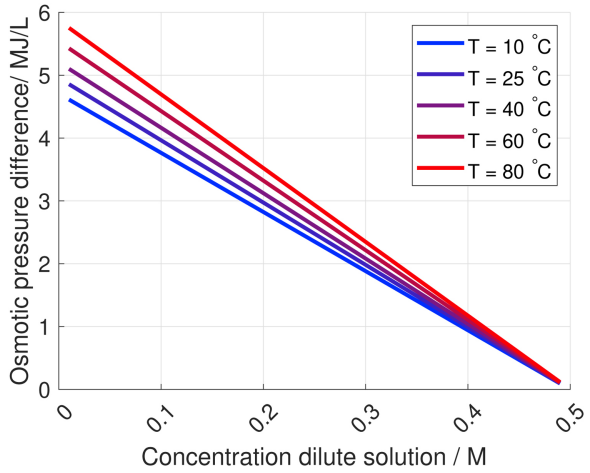


**Fig. 15.** Osmotic pressure difference for PRO and RO. $c_c = 1 - c_d$.

The pumping power consumption in the capacitive energy storage system is half of the pumping consumption in the electrolytic and osmotic energy storage system, since MCDI and CDP only have one flow compartment per unit cell. The efficiency of MCDI and CDP for different residence time at fixed temperature, $T = 25\,^{\circ}C$, is given in Fig. 21(a) and (b), while the total efficiency is given in Fig. 21(c). The efficiency for MCDI and CDP are decreasing rapidly with residence time due to the increase in power consumption of pump.

The temperature effect on the efficiency of MCDI and CDP at fixed residence time, $t_{res} = 20\,s$ is given in Fig. 22(a) and (b). The total efficiency of the membrane capacitive energy storage system is given in Fig. 22(c). The efficiency increases by elevating temperature, due to temperature dependency of drive potential, resistance and pump power consumption.

### 3.4. Energy price and membrane cost

A comparison of minimum, maximum and mean values of energy price between EU and USA are shown in Figure. 23 . The energy cost of each energy storage system needs to be competitive with the energy prices given in Fig. 23 to take its market share. A more optimistic market constraint would consider being paid to dump surplus electricity, as is seen in Europe, cf. Appendix C.

The cost of the membrane for ED and MCDI was reported two or three times higher than that for RO according to Van der Bruggen et al. [68]. Other researchers like Pirsaheb et al. [69] reported that considering the capital, operational and maintenance costs, ED membranes are more expensive than RO membranes based on a case study. For separation technology, ED has received less attraction compared to RO. Although RO membranes are cheaper than ED membranes, there are several factors which make ED more attractive compared to RO at certain conditions as reviewed by Westerling [70], reporting that ED is more tunable for specific membranes and constant flow rate. ED requires cross-flow separation using ion exchange membranes, and it operates at lower pressure range (approximately 7 bar) which requires less physical space, easier maintenance and longer lifetime compared to RO (typical range of pressure is 30–80 bar).

The capacitive and electrodialytic energy storage systems are using AEMs and CEMs; either as a separate layer or as a coating applied directly onto the electrodes. NAFION 117 is a popular membrane [60] with a cost of approximately $1\$\,cm^{-2}$ [71] ($10\,000\$\,m^{-2}$), while membranes from Fumatech is approximately $0.05\$\,cm^{-2}$ ($500\$\,m^{-2}$) at lab scale. The cost of the osmotic membrane is typically $20–50\$\,m^{-2}$ [72,17]. Post claims the electrodialytic membrane is 2–3 times more expensive than the osmotic membrane, but the installed area cost of membranes considering pump, turbine and pressure vessels, evens out this cost difference [23]. Based on a financial feasibility study of a RED power plant by Daniilidis [17], the most influential parameter on the cost is the price of the membranes. For simplicity and initial estimate, all other sources of the cost are neglected. The lifetime for all three batteries is assumed to vary from 3 to 10 years [3,16] for comparison, with 3% down-time [17]. According to the duck curve constraint, the battery is discharging approximately 3 h a day.

The peak power densities from ED-RED, RO-PRO and MCDI-CDP are given in Table 2. The total cost per total membrane area is estimated and is shown in Fig. 24 by varying the cost per membrane area, for a constant temperature of 25 °C and 60 °C and residence time of 20 s.

The maximum energy price in EU is 0.23$/kWh and in the USA 0.31$/kWh (see Fig. 23). To generate electricity below these prices by the three storage systems with an operational time of 5 years (3 h per day and 3% downtime), considering power densities given in Table 2 for 25 °C, the membrane cost needs to be lower than 2.9, 3.0, $0.31\$\,m^{-2}$ for RED, PRO and CDP respectively. Increasing the temperature to 60 °C, the membrane can cost up to 5.2, 3.7 and $0.43\$\,m^{-2}$ for RED, PRO and CDP respectively.

### 3.5. Evaluation of the three energy storage systems

The maximum peak power densities and the total efficiencies at $t_{res} = 20\,s$ for all three energy storage systems are given in Table 2.

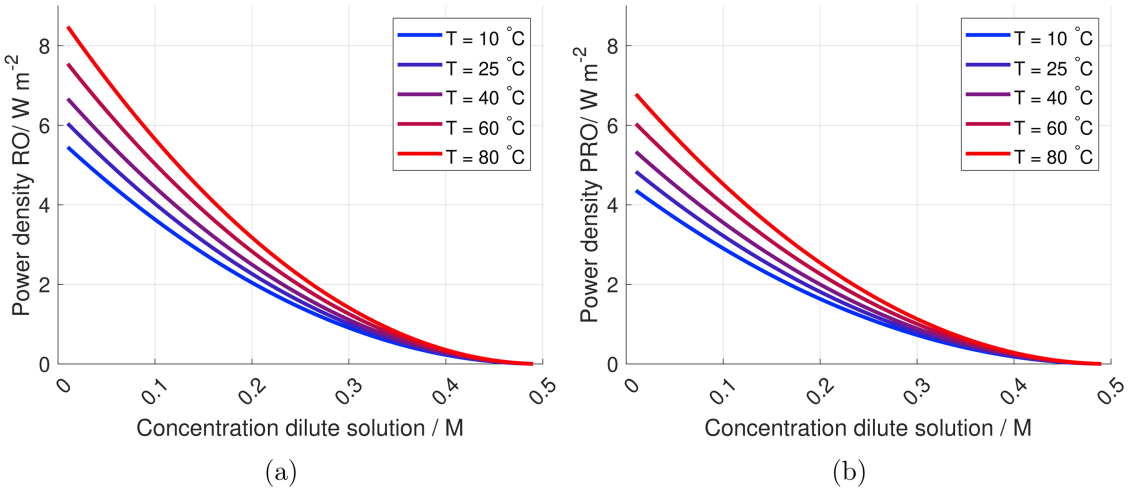


**Fig. 16.** Power per unit cell area used in RO (a) and gained from PRO (b). $c_c = 1 - c_d$.

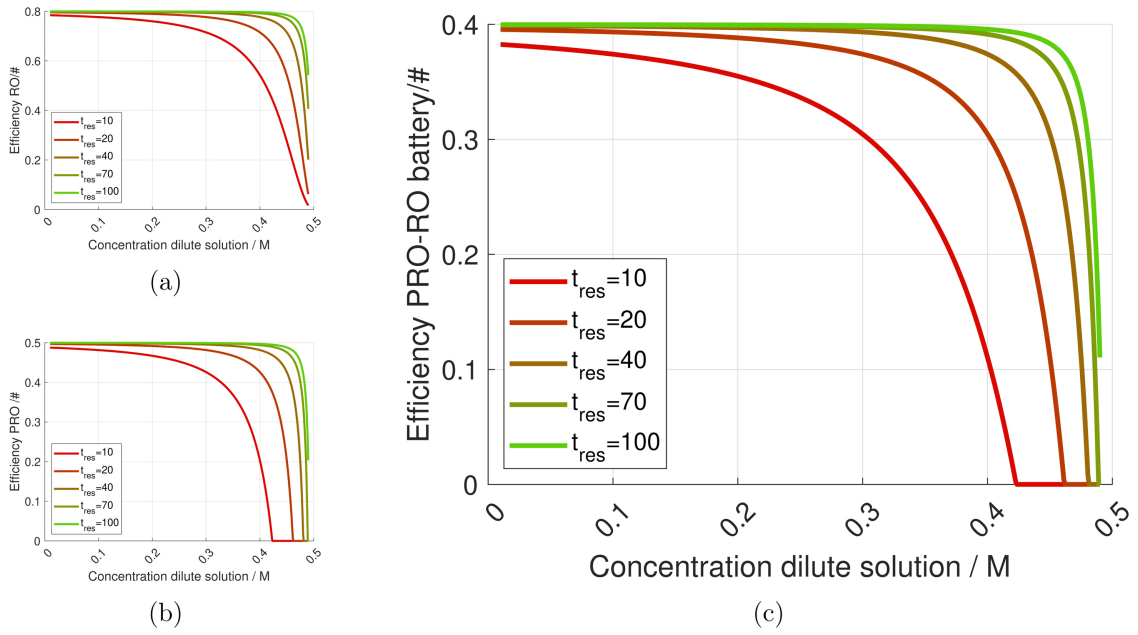


**Fig. 17.** Efficiency at different residence times for (a) RO, (b) PRO and (c) the total osmotic energy storage system. $T = 25\,^{\circ}\mathrm{C}$ and $c_c = 1 - c_d$.

*3.5.1. Power density*

The maximum power density of the electrodialytic energy storage systems is higher than the power density of the osmotic energy storage systems at temperatures over 40 °C, while the maximum power density of the capacitive energy storage system is approximately one-tenth of the power density of the other studied discharging processes.

The average discharging power density of the electrodialytic energy storage system by Kingsbury et al. [8], was in the range of 0.07–0.44 $\mathrm{W\,m^{-2}}$, which is less than the average power density of our electrodialytic energy storage system (1.7 $\mathrm{W\,m^{-2}}$ at 25 °C). The difference in power density is due to difference in the operating conditions like lower temperature (18.5 °C), lower average permselectivity (91%) and lower concentration difference (0.5 M and 0.25 M). They considered pumping losses, Faradaic losses (which is mostly influenced by osmosis) and losses in the model. It is important to mention that Kingsbury et al. [8] did the first experimental study that demonstrated that ED-RED could be used for energy storage. Also, the Kingsbury et al. study showed that by comparing experimental measurements and modelled results, the performance of the ED-RED battery could be successfully modelled based on known ED-RED and mass transport.

To maximise peak power density in the osmotic energy storage system, membrane characteristics like water permeability, the porous support and membrane structure factor are very important [4,23]. Chemical and mechanical stable materials with desirable separation capability are also desired for the RO membrane due to the operating system in high-pressure condition [50,2]. Yip et al. [50] fabricated a thin-film composite PRO membrane to find a compromise between water permeability and selectivity to maximise the peak power density to 10.0 $\mathrm{W\,m^{-2}}$ for a system containing river and sea water as feed and draw solutions, respectively. Utilising the other manufactured

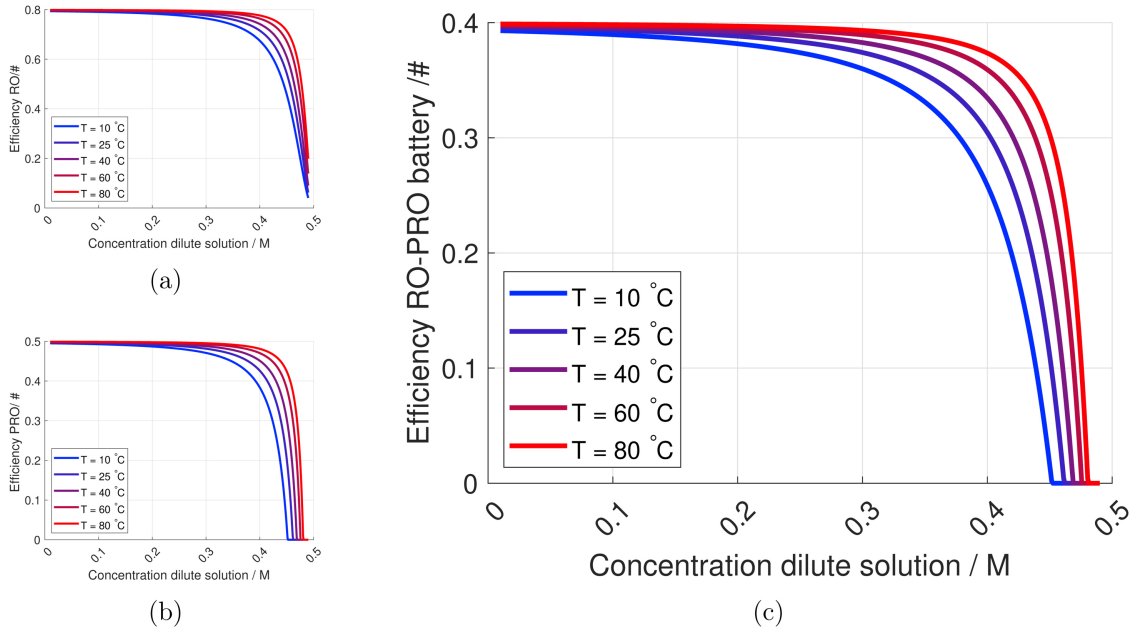


**Fig. 18.** Efficiency at different temperatures for (a) RO, (b) PRO and (c) the total osmotic energy storage system. $t_{res} = 20\,\mathrm{s}$ and $c_c = 1 - c_d$.

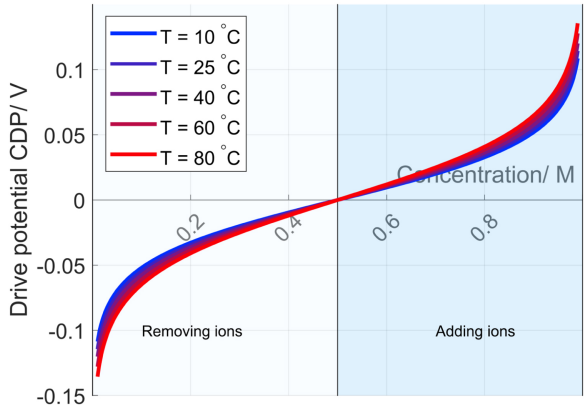


**Fig. 19.** Drive potential CDP for different temperatures.

membranes with lower salt permeability but with less water permeability resulted in reducing the peak power density as 6.1 W m$^{-2}$ at 25 °C [50]. These values are comparable with the peak power densities achieved at the studied temperature range in our work for PRO (4.83 W m$^{-2}$ at 25 °C), assuming a lower membrane water permeability in our work compared to the water permeability of membrane reported by Yip et al. [50].

One reason for the low power density in CDP is the constant current constraint considering time which is applied in the capacitive energy storage system when the current at peak power of the capacitive energy storage system should be time dependent. Liu et al. reported a maximum power density of 0.205 W m$^{-2}$ using concentration of 0.02 M and 0.5 M and a constant current [25], while Sales et al. [58] had a maximum power density of 0.060 W m$^{-2}$ with the same concentration difference as Liu et al. Hatzell et al. increased the power density from 0.5 W m$^{-2}$ to 0.9 W m$^{-2}$ using ammonium bicarbonate [60].

Another reason for the low power density in the capacitive energy storage system is the much larger unit cell resistance in MCDI-CDP compared to RO-PRO and ED-RED. Considering low power density in CDP, the electrode resistance was neglected for comparison to RED and PRO, giving maximum power densities from 1.30 to 4.10 W m$^{-2}$ at temperatures from 10 °C to 80 °C. It is important to highlight that the maximum power density while adding ions to the electrodes is at the same level as the maximum power densities in RED and higher than PRO (11.0 W m$^{-2}$ at 25 °C from CDP). This is due to lower resistance in the cell with only one compartment with a concentrated solution, leading to a higher current density (130 A m$^{-2}$ at the start of discharge at 25 °C). However, the maximum power density while removing ions in CDP at 25 °C is 1.21 W m$^{-2}$ which is low compared to the values in RED and PRO. This is due to the high resistance in the cell with only one compartment with diluted solution, leading to a lower current density (15.2 A m$^{-2}$ at the start of discharge at 25 °C). A time-weighted average of maximum power density in CDP is then lower than the maximum power densities in RED and PRO.

Despite low power density and problems with the switching time, the capacitive energy storage system has some advantages over the electrodialytic and osmotic energy storage system. The capacitive system is able to produce electric energy without the need of redox solution (see Fig. 4) used in ED-RED or auxiliary equipment such as a turbine and a pressure exchanger in RO-PRO, thus introducing fewer potential losses in the capacitive systems compared to the other two.

### 3.5.2. *Effect of temperature*

In our work, elevating the temperature from 10 °C to 80 °C, increases the power density with more than a factor of 3 for the electrodialytic discharging techniques, while the osmotic and capacitive discharging system increases with a factor 2 for the same temperature increase. The increase in the power density is due to the reduction in the solution resistance and the increase in the drive potential, as well as decreasing of the viscosity and thereby the pumping losses, at elevated temperatures.

Jalili et al. [73] performed a simulation study to investigate the effect of temperature on mass and momentum transport for a dilute channel of a RED system, documenting that increasing Re number as a result of elevated temperature, improves the mass transfer due to enhanced effective diffusivity at higher temperatures. Re number might be increased either by increasing the flow velocity which inturn increases the pressure drop across the channel or reducing the viscosity by enhancing temperature which reduces the pressure drop [73]. Increasing of the temperature can be implemented by utilising the waste heat. Luo et al. [74] and Benneker et al. [75] reported experimentally an increase of the net power density of RED by the usage of the waste heat from industrial processes. Daniilidis et al. [17] performed an experimental investigation for the energy generated by RED using brine at 5 M and reported an increase in power density of almost 80% (from 3.8 to 6.7 W m$^{-2}$), when temperature was increased from 25 °C to 60 °C. Despite the increase in power density, they also found a decrease in the perm-selectivity of the membrane at higher temperatures. The decrease in perm-selectivity with increased temperatures is something that is not considered in our model. Mei et al. [76] investigated experimentally coupling of RO as a desalination process and RED as a power production unit, but the power gained was low (0.6 W m$^{-2}$ at 60 °C).

Anastasio et al. [77] reported an increase of power density for PRO from 1.3 to 4.0 W m$^{-2}$, by increasing the temperature from 20 °C to

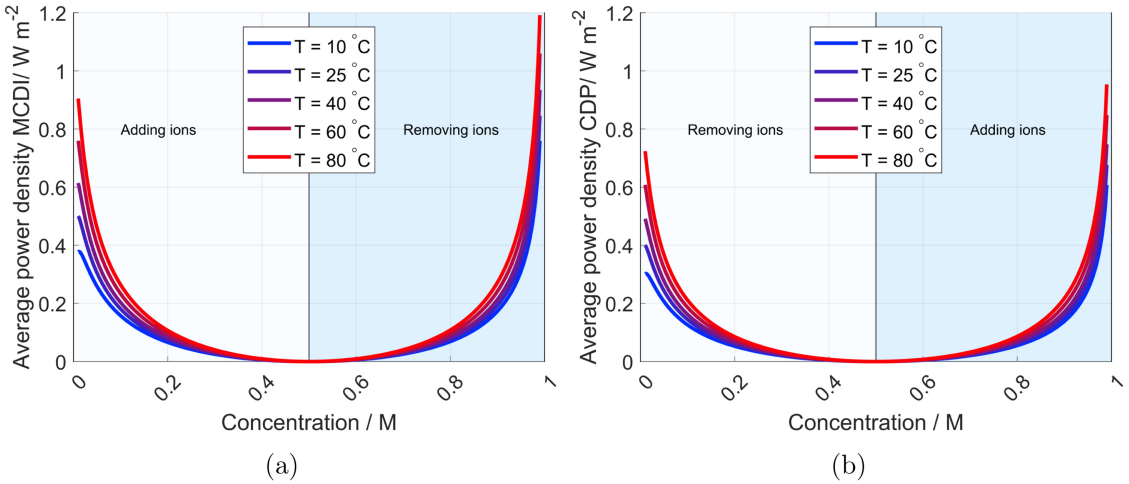


**Fig. 20.** Average power per unit cell area for adding and removing ions from electrode for MCDI (a) and CDP (b).

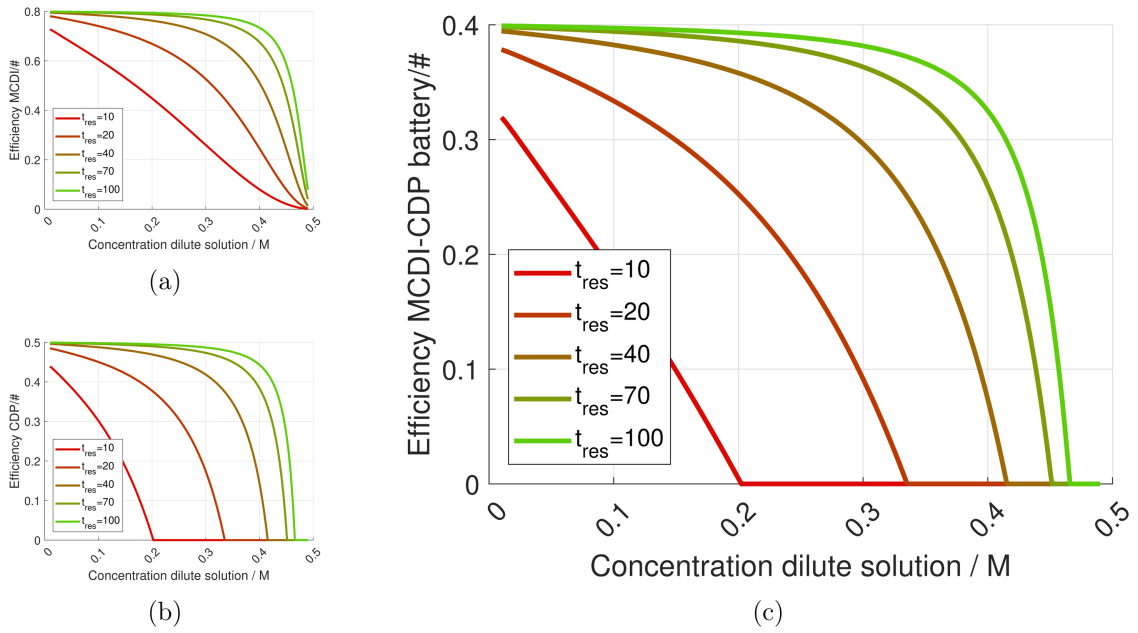


**Fig. 21.** Efficiency at different residence time for (a) MCDI, (b) CDP and (c) the total capacitive energy storage system. $T$ = 25 °C. $c_c = 1 - c_d$.

40 °C for distilled water and brine (0.5 M). It is reported by Van der Hoek et al. [78] that RO efficiency remains almost constant by temperature changes, as it is a pressure driven process. The RO performance slightly decreases by increasing the temperature due to lower salt rejection at higher temperature and temperature only influences on feed pressure. The salt rejection is not included in our model, and will lower the power density from the osmotic energy storage system. To the author's knowledge, there is no reported research for the temperature effect on the power density generated by CDP. The temperature effect on the power density of RED and PRO found from our model is comparable to the values found in the literature.

Despite enhanced power at elevated temperatures, increasing the temperature has some drawbacks such as thermal degradation of the membranes. However, membranes withstanding temperatures up to 100 °C are reported in the literature [79].

Waste heat could also be utilised in other systems, such as membrane distillation [80,81] (instead of ED) and for instance an organic Rankine cycle [82,83] for power generation. Although efficiencies for both of these technologies can be as high as 90% relative to the Carnot efficiency [81,83], they are not as easily combined into an energy storage system as those proposed here. As such, the utilisation of waste heat to increase the efficiency of the proposed systems is reasonable. It should also be noted that the consumption of waste heat would be low, as the systems are closed and could be designed with minimum heat losses.

### 3.5.3. *Efficiency*

From our model, the efficiency of all systems is increased for higher concentration differences due to the increased available potential and consequently generated energy during the discharging process. It is

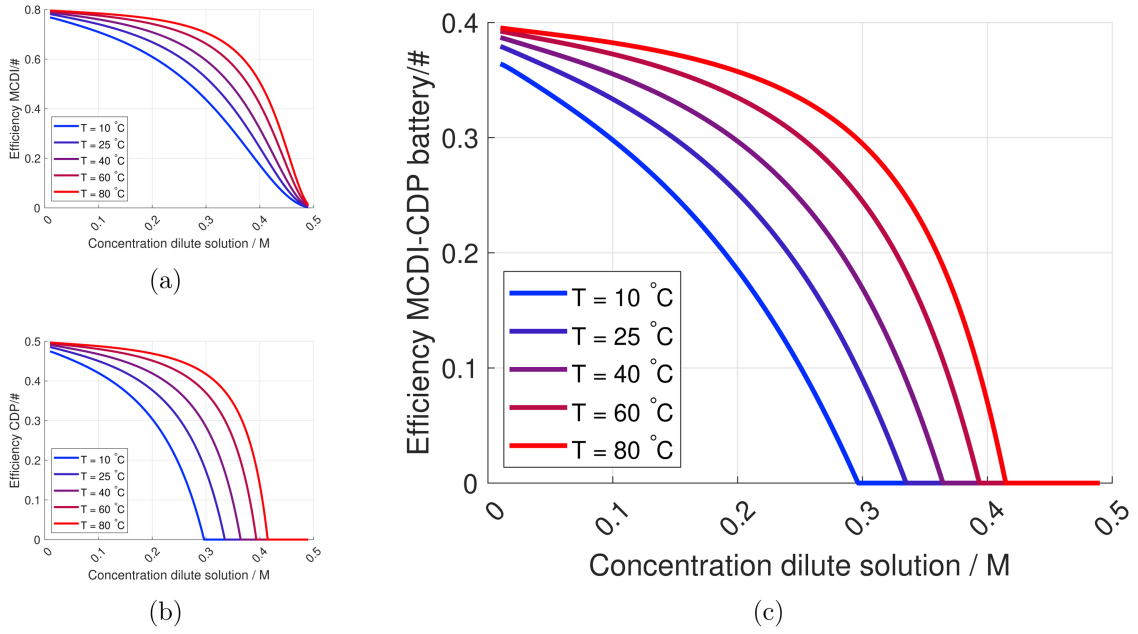


**Fig. 22.** Efficiency at different temperatures for (a) MCDI, (b) CDP and (c) the total capacitive energy storage system. $t_{res}$ = 20 s and $c_c = 1 - c_d$.

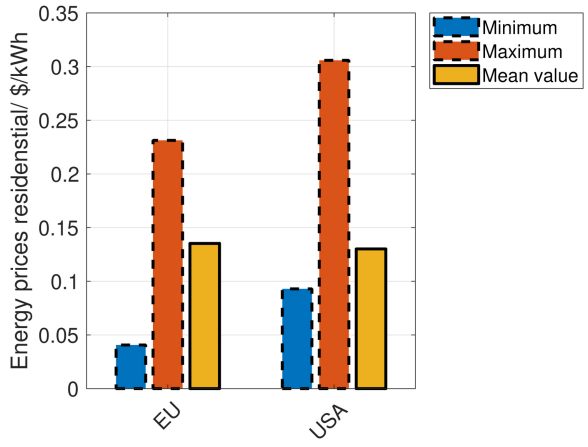


**Fig. 23.** Electricity prices for residential consumers in USA and EU, with minimum (Louisiana and Ukraine), maximum (Hawaii and Ireland) and mean values averaging over all countries or states [66,67].

important to highlight that the efficiency of the electrodialytic and capacitive energy storage systems are decreasing at lower dilute concentrations, due to the increased ohmic resistance. The relatively high pumping loss in the capacitive energy storage system compared to the power density obtained by CDP, gives a lower efficiency for this system compared to ED-RED and RO-PRO. Increasing the residence time, increases the efficiency of the three types of energy storage systems due to the decrease in pumping losses. Increasing the temperature, increases the efficiency for all systems due to reduced pumping losses and increased power densities.

Kingsbury et al. [8] defined round-trip energy efficiency as the product of current efficiency and voltage efficiency. Despite having the small ohmic loss at low current density, the rate of self-discharging is so high that it results in reducing current efficiency, which gives a low round-trip energy efficiency. At higher current densities, the high ohmic losses lead to a low voltage efficiency and thereby a low round-trip energy efficiency. For that reason, the optimum current density is between 11 and 17 $A\,m^{-2}$, where the two losses become minimised. Kingsbury et al. reported a round-trip energy efficiency between 21.2 and 34.0% by performing experiments in an electrodialytic energy storage system and neglecting the pumping loss [8]. The efficiency of our studied ED-RED energy storage system was calculated around 40% at starting of discharging and charging. Note that our model does not account losses such as concentration polarisation or osmotic losses by neglecting the water transport through the ionic exchange membranes.

In a review by Yip et al. [18], the efficiency of an energy storage system was expressed as the ratio of the extracted work to Gibbs free energy of two solutions with different salinity. They documented the efficiency of PRO for a system containing sea and river water, as 44% with an average power density of 3.7–5.2 $W\,m^{-2}$ based on a modelling assessment. However, Yip et al. have used another reference values for efficiency than what is used in our study.

For the discharging of the capacitive energy storage system, energy efficiency up to 46% is reported using wire electrodes in parallel [84].

For the charging part of the capacitive energy storage system, the efficiency is mostly given as the charge efficiency defined as the charge removed from the solution, where Agartan et al. reported an efficiency of MCDI of 49% [85].

It is worth mentioning that to the best of our knowledge; there is no reported round-trip efficiency in the literature, measured experimentally or calculated through modelling approach for RO-PRO or MCDI-CDP concentration batteries.

## 4. Conclusion

Energy storage systems utilising concentration gradients are one of the solutions to a non-toxic and cheap large-scale energy storage. The current work introduces combined salinity gradient technologies (RED, PRO and CDP) with the corresponding desalination processes (ED, RO and MCDI). Mathematical models were developed for comparing three types of energy storage systems and addressing the influential factors on the performance such as temperature or energy consumption by the pump for the same range of concentrations. Assuming the same pump specifications for all studied systems and isothermal conditions, the maximum power density of an electrodialytic energy storage system is higher than the maximum power density of an osmotic energy storage system at temperatures above 40 °C. The maximum power density of a capacitive energy storage system is approximately one-tenth of the other two systems.

The power densities of the electrodialtic energy storage system increases with more than a factor of 3 by elevating temperature from 10 °C to 80 °C, while the osmotic and capacitive energy storage systems increased by a factor 2. By increasing the temperature, the open circuit potential of ED-RED and MCDI-CDI and the osmotic pressure of RO-PRO increases. Also, the pressure loss of the pump reduces for all three systems at elevated temperature, due to reduced the viscosities. The reduction in the pumping losses at elevated temperatures indicate a potential use for waste heat. Based on our modelling assessment, the efficiencies of the electrodialytic, osmotic and capacitive storage systems are obtained as similar. Therefore, the power density and operational conditions of implementing these energy storage systems define which systems are more effective regarding energy storage.

Pumping energy consumption characterised by residence time and the temperature is another critical parameter for a salinity gradient energy storage system. Increasing the residence time by a factor 10, decreases the pumping power consumption with a factor 100, while increasing the temperature from 10 °C to 80 °C, decreases the power density consumed by pump by a factor 25. Both factors will increase the performance of energy storage systems.

A cost evaluation is presented for each technology. There is a threshold for the cost of different membranes at 5.2, 3.7 and 0.43$ $m^{-2}$ for the electrodialytic, osmotic and capacitive energy storage system, respectively, at maximum power density at 60 °C. Below this threshold, energy generation is economically feasible, although depending on the operational lifetime of the membrane, downtime, maximum power density and the average electricity price. There is a need for significant reduction of the membrane cost for storing energy through all mentioned concentration energy storage systems.

**Table 2**
$P^{max}$ for RED, PRO and CDP at $t_{res} = 20$ s and the total energy storage systems efficiencies (recall that the maximum total efficiency for the energy storage systems are 0.4).

| $T$ (°C) | $P_{RED}^{max}$ ($W\,m^{-2}$) | $P_{PRO}^{max}$ ($W\,m^{-2}$) | $P_{CDP}^{max}$ ($W\,m^{-2}$) | $\eta_{ED-RED}^{Pmax}$ # | $\eta_{RO-PRO}^{Pmax}$ # | $\eta_{MCDI-CDP}^{Pmax}$ # |
|---|---|---|---|---|---|---|
| 10 | 3.18 | 4.36 | 0.403 | 0.390 | 0.393 | 0.364 |
| 25 | 4.69 | 4.83 | 0.503 | 0.395 | 0.396 | 0.379 |
| 40 | 6.28 | 5.33 | 0.593 | 0.397 | 0.397 | 0.387 |
| 60 | 8.54 | 6.04 | 0.708 | 0.399 | 0.398 | 0.393 |
| 80 | 11.0 | 6.78 | 0.823 | 0.399 | 0.399 | 0.395 |

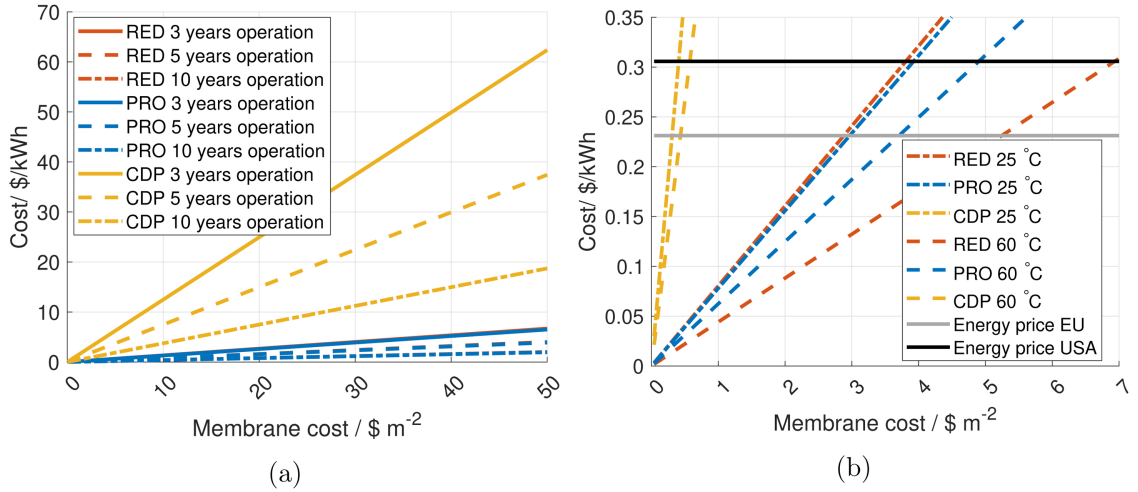


**Fig. 24.** Cost of electric energy generation ($/kWh) RED, PRO and CDP at (a) 25 °C and (b) 25 °C and 60 °C compared to the energy price in EU and USA. Residence time is 20 s. Due to the similar power density from RED and PRO at 25 °C, the lines for the two energy generating systems overlap.

**Acknowledgments**

Financial support from Norwegian University of Science and Technology (NTNU), via PhD grants and strategic research program – ENERSENSE (Energy and Sensor Systems) is greatly acknowledged. Zohreh Jalili and Kjersti Wergeland Krakhella would like to thank Vahid Alipour Tabrizy and Jens Wergeland Krakhella for all help and support throughout this work.

## Appendix A. Resistance, current density and water flux

The ohmic resistance for the unit cell and the current density at the peak power density in RED, are given in Fig. A.25. The water flux for PRO is given in Fig. A.26. The resistance of CDP and MCDI and the current density at the peak power density in CDP are given in Fig. A.27.

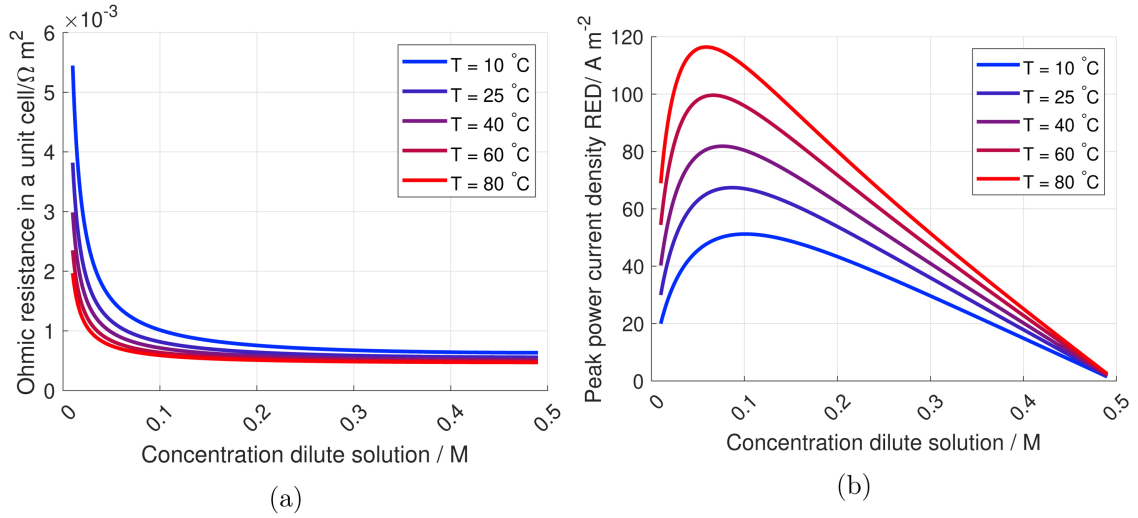


**Fig. A.25.** The figure shows the ohmic resistance of the ED-RED unit cell (a) and the current at peak power density per RED unit cell area during discharging (b). The current density during charging is considered half of the current density during discharging based on the Duck curve constraint. $c_c = 1 - c_d$.

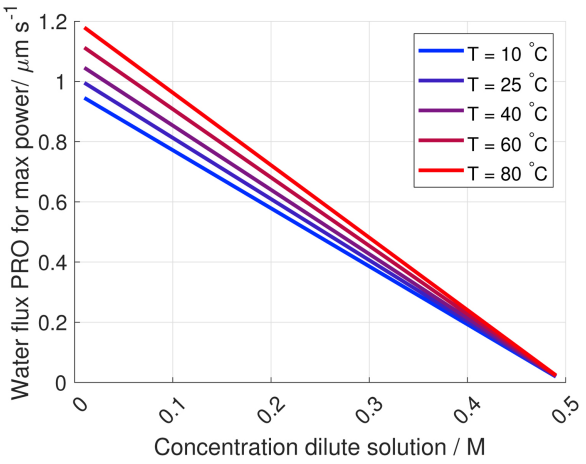


**Fig. A.26.** Water flux at maximum power density for PRO. $c_c = 1 - c_d$.

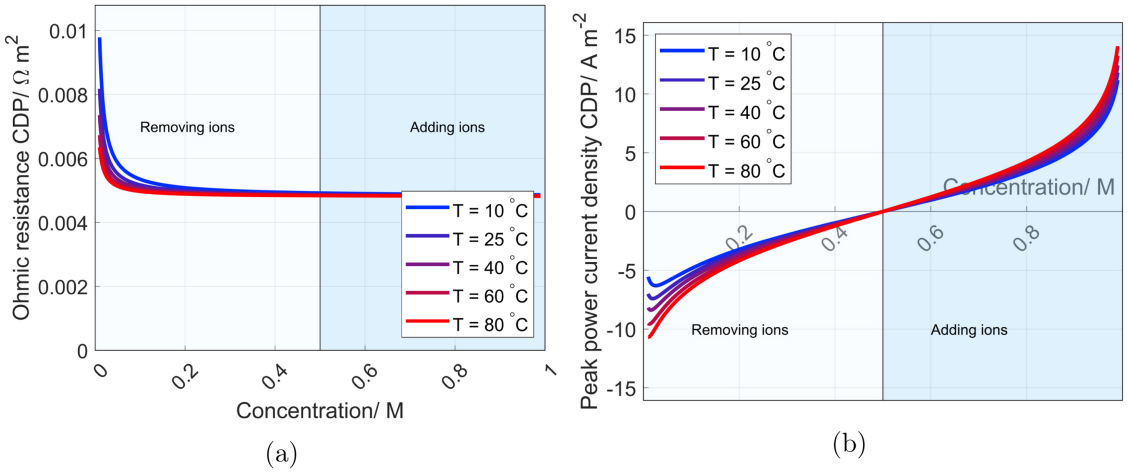


**Fig. A.27.** The figure shows the ohmic resistance in CDP and MCDI (a), and input peak power current density per unit cell area for CDP for different temperatures (b). The current density during charging is considered half of the current density during discharging for the same concentration, based on the Duck curve constraint.

## Appendix B. The relative effect of activity coefficients

The relative effect of the activity coefficients on open circuit potential for the electrolytic and capacitive energy storage system (Fig. B.28), power densities (Fig. B.29) and efficiencies of ED-RED concentration battery (Fig. B.30) at different temperatures are compared to the simplified

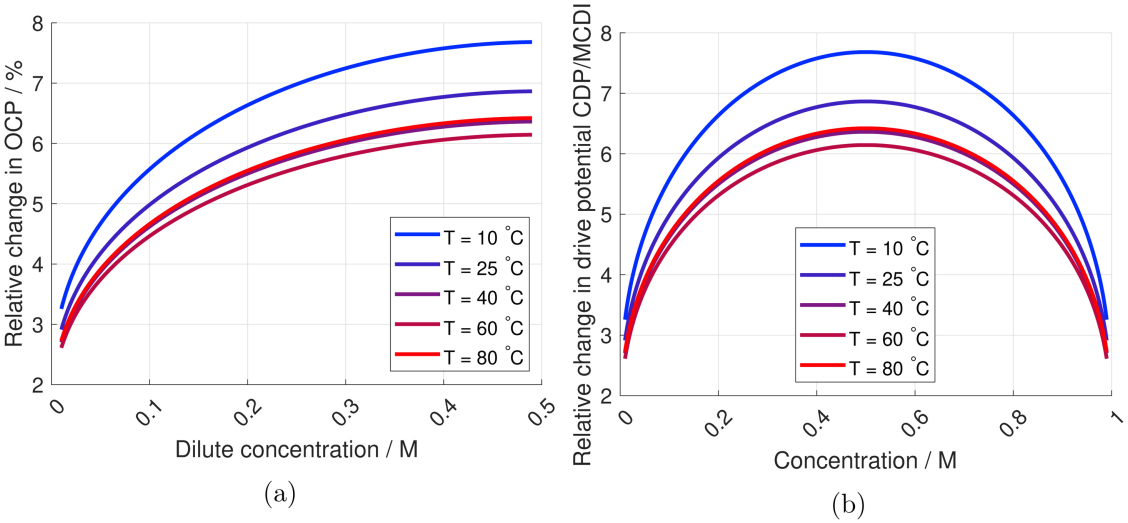


**Fig. B.28.** The figure shows the relative effect of the activity coefficients on open circuit potential of ED-RED (a) and MCDI-CDP (b) at different temperatures compared to the simplified assumption where concentrations are used instead of activity coefficients.

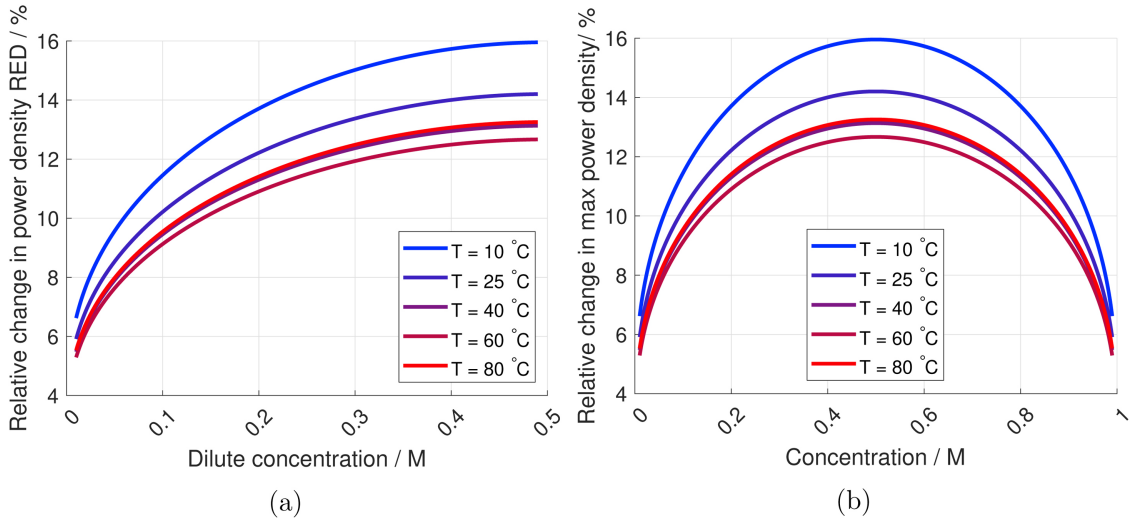


**Fig. B.29.** The figure shows the relative effect of the activity coefficients on power densities of ED-RED (a) and MCDI-CDP (b) at different temperatures compared to the simplified assumption where concentrations are used instead of activity coefficients.

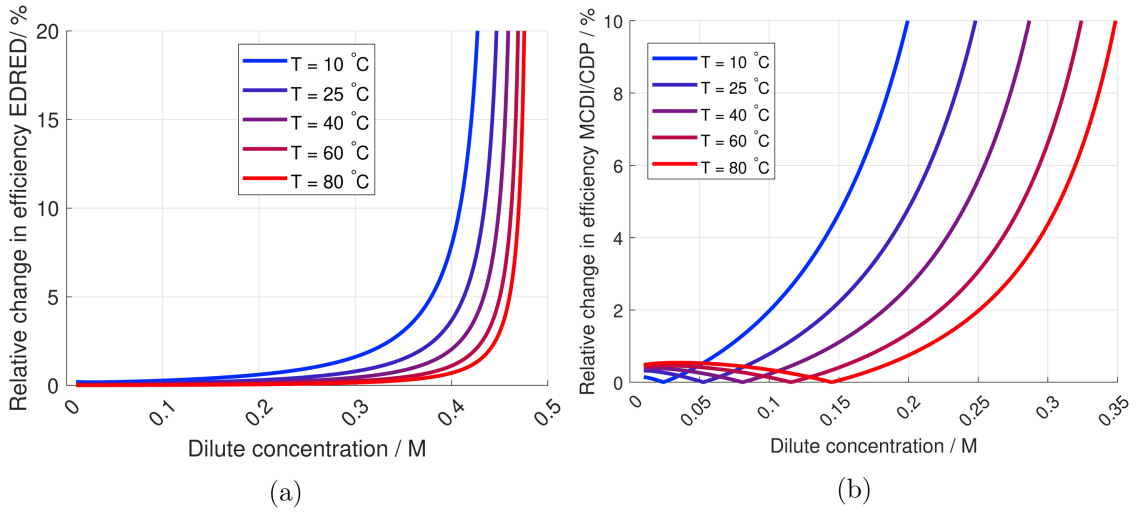


**Fig. B.30.** The figure shows the relative effect of the activity coefficients on the efficiency of ED-RED (a) and MCDI-CDP (b) at different temperatures compared to the simplified assumption where concentrations are used instead of activity coefficients.

assumption where concentrations are used instead of activity coefficients. The comparison reveals that the power density at most is changing by 16% while the efficiency is not be influenced considerably.

## Appendix C. Market case constraint

This study assumes that electricity prices are zero when charging and local high average market when discharging. This free charging and local high market price at discharge should be seen as a moderate market constraint and local low market prices represents non-interesting energy storage markets. This study assumes that electricity prices are zero when charging, and maximum market when discharging. This assumption should be seen as a moderate market constraint. A much more optimistic market constraint would consider on the one hand being paid to dump surplus electricity like seen, e.g. in Europe, where negative electricity prices at the extreme have enabled power to gas (dumping electricity into electrolysis and feeding hydrogen into the natural gas pipeline), and on the other hand, being paid twice (or more) the average electricity price. A pessimistic market constraint would be to consider charging prices half of discharging prices. To justify this, one must look at the difference in electric energy cost for industry and residential, where the industry over the years have had close to constant prices while the residents are on closed to increasing electric energy costs (see Fig. C.31). The difference in price development can be seen as a consequence partly because of the developing duck curve where larger industries can get power purchase agreements based on large volumes, steady load and high degree of predictability on the one hand whereas residential on the other hand represent small consumers with “inconvenient” consumer pattern along with several others.

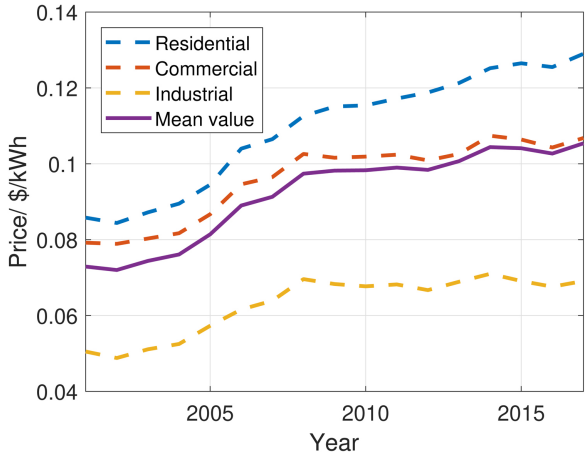


**Fig. C.31.** Energy prices for different sectors in USA from 2000 to 2017.

## Appendix D. Update beyond the review process

This review paper has been written over a long time, in addition to a lengthy review process, and new data has come out on all three energy systems alongside. This is summarised as follows.

Recent reaches state that the ideal channel height should be 200–350 μm [86,87], while Vermass et al. [62] found the optimal channel height to be less than 100 μm. Changing to 300 μm in our model lowers the maximum RED power density up to 30% and CDP up to 20%. The power density in PRO is almost independent of channel height. Correspondingly, reducing the channel height to 100 μm increases the RED power density of RED and CDP up to 60% and 20% respectively. However; since the concentration polarisation is not included in the model, the changes in the channel height does not reflect all the losses in the power density.

The ideal open area of the spacer is found to be 80% [88], and lately (2018) the ideal open area for lowering the ED energy is found to vary with current (tested for 2% and 100% [89]). Given an increase in the open area from 0.5 to 0.8 (assuming spacershadow = 1 − openarea), the RED power density increases with up to 40%, while for CDP it increased with up to 10%. PRO power density is independent of the open area.

Water permeability for osmotic membranes typically varies between 0.41 and 10 pm/(Pa s) [90,91,4], while higher values typically decrease salt rejection. A recent study [91] demonstrates a low-pressure reverse osmosis membrane showing both high water permeability (1.51 pm/(Pa s)) and a high salt rejection (96.1%). Increasing the water permeability from 0.41 to 1.51 pm/(Pa s) increases the maximum power density from PRO with 70%.

The membrane conductivity varies a lot with membrane type. Porada et al. and Güler et al. summarised properties from over 20 different ion exchange membranes, where the membrane resistance was varying between 0.8 and 17 Ω cm$^2$ [92,93]. Given a membrane resistance of 0.8 Ω cm$^2$, increase the RED and CDP power density with up to 10% and 1% respectively. Increasing the membrane resistance to 17 Ω cm$^2$ decreases the RED and CDP power density with up to 80% and 50% respectively. The membrane permselectivity decreases with concentration difference [40], but in the relevant concentration range according to this article, the permselectivity does not deviate much from 1.

It should be highlighted that this is an active field of research where the power and efficiency are always improving, further increasing the potential for these kinds of technologies.

## References

[1] R. Pattle, Production of electric power by mixing fresh and salt water in the hydroelectric pile, Nature 174 (4431) (1954) 660.
[2] J.W. Post, J. Veerman, H.V. Hamelers, G.J. Euverink, S.J. Metz, K. Nymeijer, C.J. Buisman, Salinity-gradient power: evaluation of pressure-retarded osmosis and reverse electrodialysis, J. Membr. Sci. 288 (1) (2007) 218–230.
[3] J. Post, C. Goeting, J. Valk, S. Goinga, J. Veerman, H. Hamelers, P. Hack, Towards implementation of reverse electrodialysis for power generation from salinity gradients, Desalination Water Treat. 16 (1–3) (2010) 182–193.
[4] G.Z. Ramon, B.J. Feinberg, E.M. Hoek, Membrane-based production of salinity-gradient power, Energy Environ. Sci. 4 (11) (2011) 4423–4434.
[5] DNV-GL, Energy Transition Outlook 2017, DNV-GL, 2017.
[6] O.S. Burheim, Engineering Energy Storage, Academic Press, 2017.
[7] P. Denholm, M. O'Connell, G. Brinkman, J. Jorgenson, Overgeneration from Solar Energy in California: A Field Guide to the Duck Chart, (2015).
[8] R.S. Kingsbury, K. Chu, O. Coronell, Energy storage by reversible electrodialysis: the concentration battery, J. Membr. Sci. 495 (2015) 502–516.
[9] B. Dunn, H. Kamath, J.-M. Tarascon, Electrical energy storage for the grid: a battery of choices, Science 334 (6058) (2011) 928–935.
[10] N. Boon, R. Van Roij, Blue energy from ion adsorption and electrode charging in sea and river water, Mol. Phys. 109 (7-10) (2011) 1229–1241.
[11] J. Maisonneuve, P. Pillay, C.B. Laflamme, Pressure-retarded osmotic power system model considering non-ideal effects, Renew. Energy 75 (2015) 416–424.
[12] S. Senthil, S. Senthilmurugan, Reverse osmosis-pressure retarded osmosis hybrid system: modelling, simulation and optimization, Desalination 389 (2016) 78–97.
[13] M.F.M. Bijmans, O.S. Burheim, M. Bryjak, A. Delgado, P. Hack, F. Mantegazza, S. Tenisson, H.V.M. Hamelers, CAPMIX – deploying capacitors for salt gradient power extraction, Energy Procedia 20 (2012) 108–115, https://doi.org/10.1016/j.egypro.2012.03.013.
[14] M. Fernández, R. Wagterveld, S. Ahualli, F. Liu, A. Delgado, H. Hamelers, Polyelectrolyte- versus membrane-coated electrodes for energy production by capmix salinity exchange methods, J. Power Sources 302 (2016) 387–393.
[15] M.C. Hatzell, K.B. Hatzell, B.E. Logan, Using flow electrodes in multiple reactors in series for continuous energy generation from capacitive mixing, Environ. Sci. Technol. Lett. 1 (12) (2014) 474–478.
[16] M. Turek, B. Bandura, Renewable energy by reverse electrodialysis, Desalination 205 (1–3) (2007) 67–74, https://doi.org/10.1016/j.desal.2006.04.041.
[17] A. Daniilidis, D.A. Vermaas, R. Herber, K. Nijmeijer, Experimentally obtainable energy from mixing river water, seawater or brines with reverse electrodialysis, Renew. Energy 64 (2014) 123–131.
[18] N.Y. Yip, D. Brogioli, H.V. Hamelers, K. Nijmeijer, Salinity gradients for sustainable energy: primer, progress, and prospects, Environ. Sci. Technol. 50 (22) (2016) 12072–12094.
[19] W.J. van Egmond, U.K. Starke, M. Saakes, C.J.N. Buisman, H.V.M. Hamelers, Energy efficiency of a concentration gradient flow battery at elevated temperatures, J. Power Sources 340 (2017) 71–79, https://doi.org/10.1016/j.jpowsour.2016.11.043.
[20] L. Li, P. Liu, Z. Li, X. Wang, A multi-objective optimization approach for selection of energy storage systems, Comput. Chem. Eng. 115 (2018) 213–225.
[21] E.S. Skilbred, K.W. Krakhella, I.J.M. Haga, J.G. Pharoah, M. Hillestad, G. del Alamo Serrano, O.S. Burheim, Heat to $h_2$: using waste heat to set up concentration differences for reverse electrodialysis hydrogen production, ECS Trans. 85 (2018)

147–161, https://doi.org/10.1149/08513.0147ecst.
[22] R. Lacey, Energy by reverse electrodialysis, Ocean Eng. 7 (1) (1980) 1–47.
[23] J.W. Post, Blue Energy: Electricity Production from Salinity Gradients by Reverse Electrodialysis, Wageningen University & Research, 2009.
[24] Z. Jalili, O.S. Burheim, K.E. Einarsrud, New insights into computational fluid dynamic modeling of the resistivity and overpotential in reverse electrodialysis, ECS Trans. 85 (13) (2018) 129–144.
[25] F. Liu, O. Schaetzle, B.B. Sales, M. Saakes, C.J. Buisman, H.V. Hamelers, Effect of additional charging and current density on the performance of capacitive energy extraction based on Donnan potential, Energy Environ. Sci. 5 (9) (2012) 8642–8650.
[26] O.S. Burheim, F. Liu, B.B. Sales, O. Schaetzle, C.J.N. Buisman, H.V.M. Hamelers, Faster time response by the use of wire electrodes in capacitive salinity gradient energy systems, J. Phys. Chem. C 116 (36) (2012) 19203–19210, https://doi.org/10.1021/jp306522g.
[27] P. Długołęcki, J. Dąbrowska, K. Nijmeijer, M. Wessling, Ion conductive spacers for increased power generation in reverse electrodialysis, J. Membr. Sci. 347 (1-2) (2010) 101–107.
[28] L. Gurreri, A. Tamburini, A. Cipollina, G. Micale, M. Ciofalo, Cfd prediction of concentration polarization phenomena in spacer-filled channels for reverse electrodialysis, J. Membr. Sci. 468 (2014) 133–148.
[29] A. Ahmad, K. Lau, M.A. Bakar, Impact of different spacer filament geometries on concentration polarization control in narrow membrane channel, J. Membr. Sci. 262 (1) (2005) 138–152.
[30] A. Achilli, T.Y. Cath, A.E. Childress, Power generation with pressure retarded osmosis: an experimental and theoretical investigation, J. Membr. Sci. 343 (1-2) (2009) 42–52.
[31] S. Lin, A.P. Straub, M. Elimelech, Thermodynamic limits of extractable energy by pressure retarded osmosis, Energy Environ. Sci. 7 (8) (2014) 2706–2714.
[32] A.P. Straub, A. Deshmukh, M. Elimelech, Pressure-retarded osmosis for power generation from salinity gradients: is it viable? Energy Environ. Sci. 9 (1) (2016) 31–48.
[33] I. Sutzkover, D. Hasson, R. Semiat, Simple technique for measuring the concentration polarization level in a reverse osmosis system, Desalination 131 (1–3) (2000) 117–127.
[34] S. Sablani, M. Goosen, R. Al-Belushi, M. Wilf, Concentration polarization in ultrafiltration and reverse osmosis: a critical review, Desalination 141 (3) (2001) 269–289.
[35] S. Kim, E.M. Hoek, Modeling concentration polarization in reverse osmosis processes, Desalination 186 (1–3) (2005) 111–128.
[36] A. Altaee, J. Zou, A.A. Alanezi, A.H. Hawari, Osmotic power plant: Process innovation and future potential, Recent Adv. Petrochem. Sci. 7 (3) (2018).
[37] A. Altaee, J. Zhou, A. Alhathal Alanezi, G. Zaragoza, Pressure retarded osmosis process for power generation: feasibility, energy balance and controlling parameters, Appl. Energy 206 (August) (2017) 303–311, https://doi.org/10.1016/j.apenergy.2017.08.195.
[38] S. Loeb, F. Van Hessen, D. Shahaf, Production of energy from concentrated brines by pressure-retarded osmosis: II. Experimental results and projected energy costs, J. Membr. Sci. 1 (1976) 249–269.
[39] G.D. Mehta, Further results on the performance of present-day osmotic membranes in various osmotic regions, J. Membr. Sci. 10 (1) (1982) 3–19.
[40] A. Zlotorowicz, R.V. Strand, O.S. Burheim, Ø. Wilhelmsen, S. Kjelstrup, The permselectivity and water transference number of ion exchange membranes in reverse electrodialysis, J. Membr. Sci. 523 (2017) 402–408, https://doi.org/10.1016/j.memsci.2016.10.003.
[41] D.A. Vermaas, E. Guler, M. Saakes, K. Nijmeijer, Theoretical power density from salinity gradients using reverse electrodialysis, Energy Procedia 20 (2012) 170–184.
[42] A. Daniilidis, R. Herber, D.A. Vermaas, Upscale potential and financial feasibility of a reverse electrodialysis power plant, Appl. Energy 119 (2014) 257–265.
[43] J. Kim, M. Wilf, J.-S. Park, J. Brown, Boron rejection by reverse osmosis membranes: national reconnaissance and mechanism study-phase 1, Tech. Rep. Georgia Institute of Technology, 2006.
[44] H. Strathmann, Electrodialysis, a mature technology with a multitude of new applications, Desalination 264 (3) (2010) 268–288.
[45] S. Pawlowski, T. Rijnaarts, M. Saakes, K. Nijmeijer, S. Crespo, Velizarov, Improved fluid mixing and power density in reverse electrodialysis stacks with Chevron-profiled membranes, J. Membr. Sci. 531 (2017) 111–121.
[46] M. Tedesco, A. Cipollina, A. Tamburini, I.D.L. Bogle, G. Micale, A simulation tool for analysis and design of reverse electrodialysis using concentrated brines, Chem. Eng. Res. Des. 93 (2015) 441–456, https://doi.org/10.1016/j.cherd.2014.05.009.
[47] Schlumberger, Resistivity of NaCl Solutions, (2017) URL https://www.google.no/url?sa=t&rct=j&q=&esrc=s&source=web&cd=1&ved=0ahUKEwirYax3KnXAhXJLFAKHRQWAnsQFggqMAA&url=http%3A%2F%2Fwww1.uis.no%2FFag%2FLearningspace_kurs%2FPetBachelor%2Fwebpage%2Ftech%255CSchlumberger%2520charts%255C01_gen_1-1_1-5.p3.pdf&usg=AOvVaw11luS4F6p350Tr_iIh0HkD.
[48] E. ToolBox, Density of aqueous solutions of inorganic sodium salts. URL https://www.engineeringtoolbox.com/density-aqueous-solution-inorganic-sodium-salt-concentration-d_1957.html (accessed: November 2018).
[49] T. Thorsen, T. Holt, Finding hidden energy in membrane processes, Filtrat. Separ. 42 (3) (2005) 28–30.
[50] N.Y. Yip, A. Tiraferri, W.A. Phillip, J.D. Schiffman, L.A. Hoover, Y.C. Kim, M. Elimelech, Thin-film composite pressure retarded osmosis membranes for sustainable power generation from salinity gradients, Environ. Sci. Technol. 45 (10) (2011) 4360–4369, https://doi.org/10.1021/es104325z.
[51] A. Achilli, J.L. Prante, N.T. Hancock, E.B. Maxwell, A.E. Childress, Experimental results from RO-PRO: a next generation system for low-energy desalination, Environ. Sci. Technol. 48 (11) (2014) 6437–6443.
[52] D. Brogioli, Extracting renewable energy from a salinity difference using a capacitor, Phys. Rev. Lett. 103 (5) (2009) 31–34, https://doi.org/10.1103/PhysRevLett.103.058501.
[53] CAPMIX – Coordinator: Dr. IR. Martijn Bijmans, The Capacitive Principle, (2012) URL http://www.capmix.eu/project-description/the-capacitive-principle.
[54] S. Porada, D. Weingarth, H.V. Hamelers, M. Bryjak, V. Presser, P. Biesheuvel, Carbon flow electrodes for continuous operation of capacitive deionization and capacitive mixing energy generation, J. Mater. Chem. A 2 (24) (2014) 9313–9321.
[55] D. Caudle, J. Tucker, J. Cooper, B. Arnold, A. Papastamataki, Electrochemical demineralization of water with carbon electrodes: research and development progress, United States Department of the Interior, 1966, p. 190.
[56] Y. Oren, Capacitive deionization (cdi) for desalination and water treatment – past, present and future (a review), Desalination 228 (1) (2008) 10–29.
[57] S. Porada, R. Zhao, A. Van Der Wal, V. Presser, P. Biesheuvel, Review on the science and technology of water desalination by capacitive deionization, Prog. Mater. Sci. 58 (8) (2013) 1388–1442.
[58] B.B. Sales, M. Saakes, J.W. Post, C.J.N. Buisman, P.M. Biesheuvel, H.V.M. Hamelers, Direct power production from a water salinity difference in a membrane-modified supercapacitor flow cell, Environ. Sci. Technol. 44 (14) (2010) 5661–5665, https://doi.org/10.1021/es100852a.
[59] R. Rica, R. Ziano, D. Salerno, F. Mantegazza, R. van Roij, D. Brogioli, Capacitive mixing for harvesting the free energy of solutions at different concentrations, Entropy 15 (4) (2013) 1388–1407, https://doi.org/10.3390/e15041388.
[60] M.C. Hatzell, R.D. Cusick, B.E. Logan, Capacitive mixing power production from salinity gradient energy enhanced through exoelectrogen-generated ionic currents, Energy Environ. Sci. 7 (3) (2014) 1159–1165.
[61] O. Burheim, B. Sales, O. Schaetzle, F. Liu, H. Hamelers, Auto generative capacitive mixing for power conversion of sea and river water by the use of membranes, ASME 2011 International Mechanical Engineering Congress and Exposition, American Society of Mechanical Engineers, 2011, pp. 483–492.
[62] D.A. Vermaas, M. Saakes, K. Nijmeijer, Doubled power density from salinity gradients at reduced intermembrane distance, Environ. Sci. Technol. 45 (16) (2011) 7089–7095, https://doi.org/10.1021/es2012758.
[63] F.C. Store, fumasep FAS-30, (2018) URL http://www.fuelcellstore.com/fumasep-fas-30.
[64] F.C. Store, fumasep FKS-30, (2018) URL http://www.fuelcellstore.com/fumasep-fks-30?search=fks%2030.
[65] B.B. Sales, F. Liu, O. Schaetzle, C.J. Buisman, H.V. Hamelers, Electrochemical characterization of a supercapacitor flow cell for power production from salinity gradients, Electrochim. Acta 86 (2012) 298–304.
[66] Electricity Price Statistics, URL http://ec.europa.eu/eurostat/statistics-explained/index.php/Electricity_price_statistics (accessed: 10.9.2017).
[67] Table 5.6.a. Average price of electricity to ultimate customers by end-use sector, URL https://www.eia.gov/electricity/monthly/epm_table_grapher.php?t=epmt_5_06_a (accessed: 10.9.2017).
[68] B. Van der Bruggen, C. Vandecasteele, Modelling of the retention of uncharged molecules with nanofiltration, Water Res. 36 (5) (2002) 1360–1368.
[69] M. Pirsaheb, T. Khosravi, K. Sharafi, M. Mouradi, Comparing operational cost and performance evaluation of electrodialysis and reverse osmosis systems in nitrate removal from drinking water in Golshahr, Mashhad, Desalination Water Treat. 57 (12) (2016) 5391–5397.
[70] ED vs. RO: The Benefits Of Electrodialysis For Desalination, https://www.wateronline.com/doc/ed-vs-ro-the-benefits-of-electrodialysis-for-desalination-0001 (accessed: 27.6.2018).
[71] Nafion Westerling Perfluorinated Membrane, http://www.sigmaaldrich.com/catalog/product/aldrich/274674?lang=en&region=NO (accessed: 7.2.2016).
[72] A. Achilli, A.E. Childress, Pressure retarded osmosis: from the vision of Sidney Loeb to the first prototype installation – review, Desalination 261 (3) (2010) 205–211, https://doi.org/10.1016/j.desal.2010.06.017.
[73] Z. Jalili, J.G. Pharoah, O. Stokke Burheim, K.E. Einarsrud, Temperature and velocity effects on mass and momentum transport in spacer-filled channels for reverse electrodialysis: a numerical study, Energies 11 (8) (2018).
[74] X. Luo, X. Cao, Y. Mo, K. Xiao, X. Zhang, P. Liang, X. Huang, Power generation by coupling reverse electrodialysis and ammonium bicarbonate: implication for recovery of waste heat, Electrochem. Commun. 19 (2012) 25–28.
[75] A.M. Benneker, T. Rijnaarts, R.G. Lammertink, J.A. Wood, Effect of temperature gradients in (reverse) electrodialysis in the ohmic regime, J. Membr. Sci. 548 (2018) 421–428, https://doi.org/10.1016/j.memsci.2017.11.029 URL http://www.sciencedirect.com/science/article/pii/S0376738817327394.
[76] Y. Mei, C.Y. Tang, Co-locating reverse electrodialysis with reverse osmosis desalination: synergies and implications, J. Membr. Sci. 539 (March) (2017) 305–312, https://doi.org/10.1016/j.memsci.2017.06.014.
[77] D.D. Anastasio, J.T. Arena, E.A. Cole, J.R. McCutcheon, Impact of temperature on power density in closed-loop pressure retarded osmosis for grid storage, J. Membr. Sci. 479 (2015) 240–245, https://doi.org/10.1016/j.memsci.2014.12.046.
[78] J. Van der Hoek, D. Rijnbende, C. Lokin, P. Bonne, M. Loonen, J. Hofman, Electrodialysis as an alternative for reverse osmosis in an integrated membrane system, Desalination 117 (1) (1998) 159–172.
[79] J. Fan, A.G. Wright, B. Britton, T. Weissbach, T.J. Skalski, J. Ward, T.J. Peckham, S. Holdcroft, Cationic polyelectrolytes, stable in 10 m Kohaq at 100 °C, ACS Macro Lett. 6 (10) (2017) 1089–1093.
[80] S. Mrayed, D. Maccioni, G. Leslie, Efficiency of membrane distillation to produce fresh water, Int. J. Chem. Mol. Nucl. Mater. Metall. Eng. 7 (12) (2013) 991–995.

[81] X. Zhang, Y. Liu, X. Wen, C. Li, X. Hu, Low-grade waste heat driven desalination with an open loop heat pipe, Energy 163 (2018) 221–228.
[82] V. Chintala, S. Kumar, J.K. Pandey, A technical review on waste heat recovery from compression ignition engines using organic rankine cycle, Renew. Sustain. Energy Rev. 81 (2018) 493–509.
[83] B.-S. Park, M. Usman, M. Imran, A. Pesyridis, Review of organic Rankine cycle experimental data trends, Energy Convers. Manage. 173 (2018) 679–691.
[84] F. Liu, T.F. Donkers, R.M. Wagterveld, O. Schaetzle, M. Saakes, C.J. Buisman, H.V. Hamelers, Parallel up-scaling of capacitive mixing (capmix) system enhances the specific performance, Electrochim. Acta 187 (2016) 104–112.
[85] L. Agartan, B. Akuzum, T. Mathis, K. Ergenekon, E. Agar, E.C. Kumbur, Influence of thermal treatment conditions on capacitive deionization performance and charge efficiency of carbon electrodes, Sep. Purif. Technol. 202 (2018) 67–75.
[86] S.R. Shah, N.C. Wright, P.A. Nepsky, A.G. Winter, Cost-optimal design of a batch electrodialysis system for domestic desalination of brackish groundwater, Desalination 443 (May) (2018) 198–211, https://doi.org/10.1016/j.desal.2018.05.010.
[87] K.M. Chehayeb, D.M. Farhat, K.G. Nayar, J.H. Lienhard, Optimal design and operation of electrodialysis for brackish-water desalination and for high-salinity brine concentration, Desalination 420 (June) (2017) 167–182, https://doi.org/10.1016/j.desal.2017.07.003.
[88] H.-K. Kim, M.-S. Lee, S.-Y. Lee, Y.-W. Choi, N.-J. Jeong, C.-S. Kim, High power density of reverse electrodialysis with pore-filling ion exchange membranes and a high-open-area spacer, J. Mater. Chem. A 3 (31) (2015) 16302–16306.
[89] S. Porada, W.J. van Egmond, J.W. Post, M. Saakes, H.V. Hamelers, Tailoring ion exchange membranes to enable low osmotic water transport and energy efficient electrodialysis, J. Membr. Sci. 552 (February) (2018) 22–30, https://doi.org/10.1016/j.memsci.2018.01.050.
[90] Z.L. Cheng, X. Li, T.-S. Chung, The forward osmosis-pressure retarded osmosis (FO-PRO) hybrid system: a new process to mitigate membrane fouling for sustainable osmotic power generation, J. Membr. Sci. 559 (2018) 63–74.
[91] T. Yang, C.F. Wan, J. Xiong, T.-S. Chung, Pre-treatment of wastewater retentate to mitigate fouling on the pressure retarded osmosis (PRO) process, Sep. Purif. Technol. (2019).
[92] S. Porada, W. van Egmond, J. Post, M. Saakes, H. Hamelers, Tailoring ion exchange membranes to enable low osmotic water transport and energy efficient electrodialysis, J. Membr. Sci. 552 (2018) 22–30.
[93] E. Güler, R. Elizen, D.A. Vermaas, M. Saakes, K. Nijmeijer, Performance-determining membrane properties in reverse electrodialysis, J. Membr. Sci. 446 (2013) 266–276.
[94] Y.D. Raka, H. Karoliussen, K.M. Lien, O.S. Burheim, Opportunities and challenges for thermally driven hydrogen production using reverse electrodialysis system, Int. J. Hydro. Energy (2019) revised manuscript.